國 立 交 通 大 學

光電工程研究所

碩 士 論 文

飛秒脈衝整型技術於兆赫波時析光譜儀之研究

A Study of Terahertz Time Domain Spectroscopy using Femtosecond

Pulse Shaping Technology

研 究 生：林俞良

指導教授：潘犀靈 教授

中 華 民 國 九 十 八 年 七 月

飛秒脈衝整型技術於兆赫波時析光譜儀之研究

A Study of Terahertz Time Domain Spectroscopy using Femtosecond

Pulse Shaping Technology
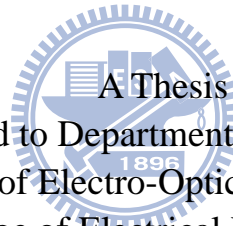
研 究 生：林 俞 良 　　　　　　　Student：Yu-Liang Lin

指導教授：潘 犀 靈 教授 　　　　　Advisor：Ci-Ling Pan

國 立 交 通 大 學

光 電 工 程 研 究 所

碩 士 論 文

A Thesis
Submitted to Department of Photonics &
Institute of Electro-Optical Engineering
College of Electrical Engineering
National Chiao Tung University
in partial Fulfillment of the Requirements
for the Degree of
Master
in

Electro-Optical Engineering

July 2009

Hsinchu, Taiwan, Republic of China

中 華 民 國 九 十 八 年 七 月

飛秒脈衝整型技術於兆赫波時析光譜儀之研究

研究生：林俞良　　　　　　　　　　　　指導教授：潘犀靈 教授

國立交通大學光電工程研究所　碩士班

摘　　要

在本論文中，我們使用飛秒脈衝雷射整形技術研究鎖模雷射中之啾頻對於產生及偵測兆赫波輻射之影響。實驗結果發現，在兆赫輻射產生端，利用些微之正啁啾光來激發兆赫波光導天線會得到較強之兆赫波輸出，且具有較寬之頻譜。在偵測端，使用零色散之最短脈衝來偵測會得到最高之時域最大值，而且具有正負色散不對稱性之行為。我們使用一維 Drude-Lorentz 模型來模擬兆赫輻射的產生和偵測過程，藉此分析驗證我們的實驗結果。最後，我們使用此同調控制兆赫波時析光譜儀來研究若干樣本在兆赫波頻段之特性，如金屬孔洞陣列，乳糖及石英。我們並討論利用光導天線對進行兆赫波時析頻譜研究時可能會導致之偵測效應。實驗證明我們使用此同調控制之兆赫波時析光譜儀可以比一般的兆赫波時析光譜儀獲得較可信賴之光學常數。

A Study of Terahertz Time Domain Spectroscopy using Femtosecond Pulse Shaping Technology

Student : Yu-Liang Lin   Advisor : Prof. Ci-Ling Pan

Institute of Electro-Optical Engineering

College of Electrical Engineering and Computer Science

National Chaio Tung Unversity

Abstract

In this thesis, we utilize femtosecond laser pulse shaping technology to study the role of chirp in generation and detection mechanism of Terahertz pulses with LT-GaAs photoconductive antenna. Experimental results show that the PC antenna excited with slightly up-chirped laser will generate THz pulses with higher peak amplitude, total power and broader bandwidth. In the detection process, similar behaviors have been observed. We use one dimensional Drude-Lorentz model to simulate THz generation and detection processes to analysis our experiment results. Finally, we use this coherently controlled THz-Time Domain Spectrometer to study the properties of several samples, such as fused silica, metal hole array and lactose. Experimental results show that we can utilize this spectrometer to get more reliable optical constants than the conventional approach.

誌　　謝

　　首先誠摯的感謝指導老師潘犀靈教授，老師悉心的教導使我得以一窺超快雷射領域的深奧，不時的討論並指點我正確的方向，使我在這些年中獲益匪淺。老師對學問的嚴謹更是我學習的典範。

　　本論文的完成另外亦得感謝口試委員黃中堯教授、趙如蘋教授與李晁達教授對於論文給予意見和指正。在研究上，特別感謝中山大學光電所的李晁達教授大力協助，因為有您的幫忙，使得本論文能夠更完整而嚴謹。

　　感謝 Mika、Moya、胎哥學長在實驗方面提供了相當大的協助，不厭其煩的指出我研究中的缺失，且總能在我迷惘時為我解惑。也感謝阿閃哥、Choppy 同學的幫忙，恭喜大家順利畢業。學弟 Sense、冠儒及睿茵學姐，你們的幫忙及搞笑我銘感在心。
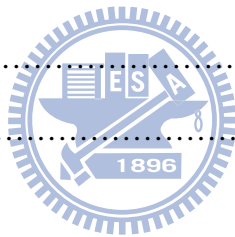
　　女友怡君在背後的默默支持更是我前進的動力，謝謝妳陪伴我渡過在風城六年的日子。最後，謹以此文獻給所以幫助過我的人及我摯愛的雙親。
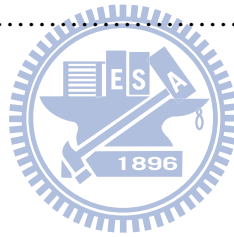
<div align="right">

2009.7.29 于 交大

</div>

Table of Contents

List of Figures

List of Tables

Chapter 1 Introduction

1.1 Introduction to Terahertz Technology

Terahertz (THz, 10^{12} Hz) wave, THz pulse, or so called T-ray, is the most interesting and important research topic recently [1-2]. It's corresponding to the frequency range from 0.1 to 10THz, wavelength range from 30 μm to 3 mm. This frequency range, as shown in Figure 1-1, has several names : far infrared, sub-millimeter wave and terahertz range. This frequency range of electromagnetic spectrum is of great important due to the rich chemical and physical processes, such as acceptor and donor in semiconductor, crystalline phonon vibrations in solid, vibrated or rotational energy level of most molecules.
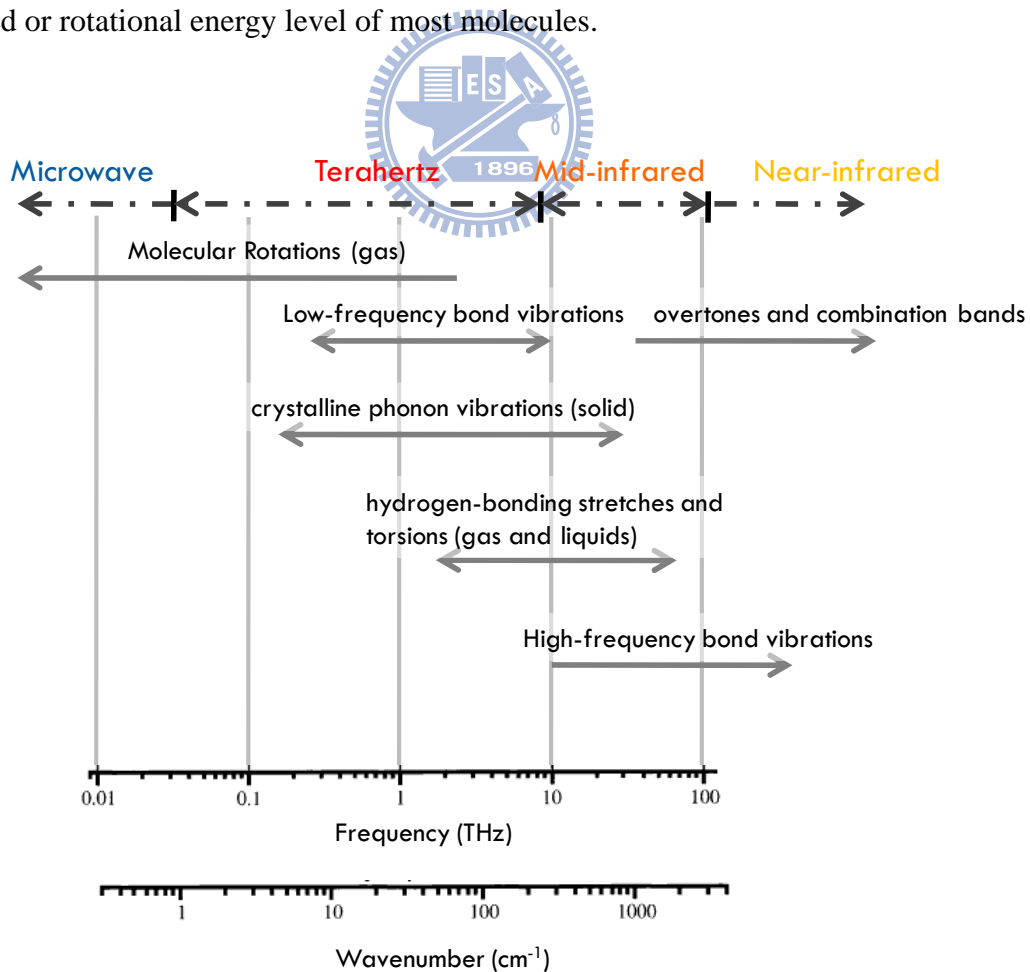
Figure 1-1 The electromagnetic spectrum in the THz region.

The electromagnetic spectrum can be divided into two parts briefly, (1) radio/microwave, and (2) light/optics. The radio wave and microwave can be generated direly through the acceleration of electronic devices (up to about 100GHz), and in the optical range, high power and coherent lasers has been well developed. In the high frequency region, X-ray can be generated from high energy accelerators. The THz regime is located at the interface of microwave electronics and infrared optics. Due to lack of suitable sources of THz waves, this regime forms "Terahertz-gap" in the electromagnetic spectrum until the mid-80s.

Thanks to the revolutionary developments of ultrashort pulse lasers in the 1990s, the first sub-100fs solid-state laser was developed by Spence et.al in 1991 [3]. In 1999, mode-locking techniques are effective over such a large bandwidth that the resulting pulses can have a duration of 6 fs or shorter [4]. With the ultrashort pulses incident into suitable semiconductor materials, the electron-hole pairs will be generated quickly, results photocurrent pulses, this acceleration/deceleration processes will generate electromagnetic waves, with frequency lies in the THz range. In 1980, Auston [5] successfully used the photoconductive dipole antenna to generate and detect coherently terahertz radiation in time domain, and this technology is called terahertz time-domain spectroscopy (THz-TDS). Other terahertz radiation generation methods, such as optical rectification [6-7], surge current in semiconductor surface [8], had been investigated.

1.2 Motivation

The phase of the femtosecond laser pulses is very important in many applications of coherent control experiments, the second order spectra phase of the pulse, also called chirp, is the dominant key in the experiment, it can be will tailored with femtosecond pulse shaping

systems. From the previous study in our group [9-10], the role of chirp pulses in the generation process of terahertz field with LT-GaAs PC antenna has been studied by C.J. Chuang [9], and the carrier dynamics in LT-GaAs was well discussed by S.H. Lin [10]. Lin found the interesting behaviors between the carrier life time and chirps as shown in Figure 1-2.
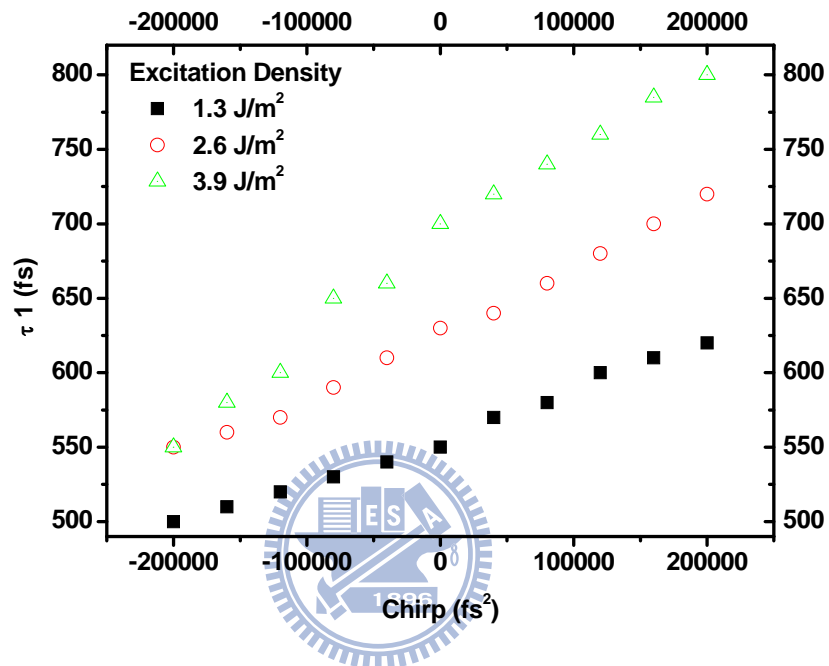
Figure 1-2 Relationship between carrier trapping of LT-GaAs and chirp under different excitation densities [10].

In additional to understand the role of chirp on Terahertz Time Domain System, S.H. Lin buildup a chirp-controlled THz-TDS to study the THz generation and detection mechanism as shown in Figure 1-3. However, this system cannot study the actual generation and detection mechanism directly, because the chirp-controlled system is in front of the THz-Time Domain System, both pump pulse and probe pulse were modified with the pulse shaper simultaneously.
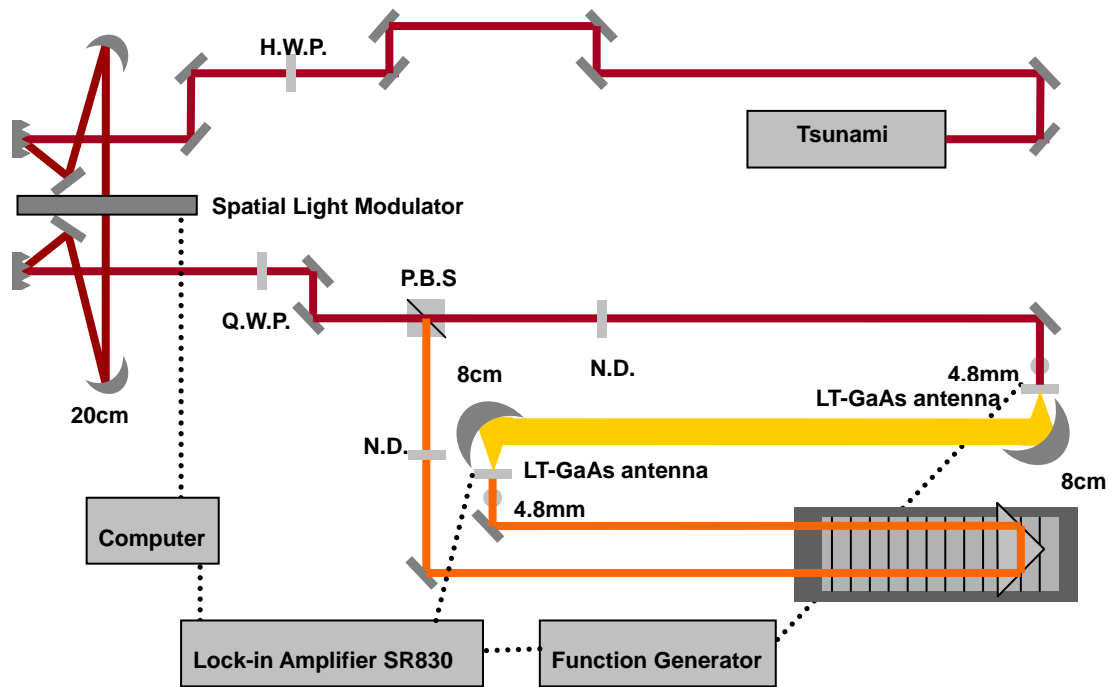
Figure 1-3 Experimental setup of chirp-controlled THz-TDS [10].

Based on Lin's study, we build-up a chirp-controlled THz-TDS, which can control only pump pulse or probe pulse respectively, it can be used to study actual influence of chirp on the generation and detection process, moreover, we use this chirp-controlled system to study the sampling effect on THz-Time Domain Spectroscopy, which is discussed in Ch4.

1.3 Organization of this thesis

An overview of THz radiation and motivation of this study are presented in chapter 1. In chapter 2, we will introduce the theories of terahertz generation and detection via PC antenna, and the simulation results of THz generation and detection is included. In chapter 3, we will demonstrate the experiment results of THz pulses generation and detection under different chirped pulses. In chapter 4, we utilize this chip-controlled THz-TDS to study the sampling effect on THz-Spectroscopy. In chapter 5, the brief conclusion and future works are presented.

References

[1] B. Ferguson, and X.-C. Zhang, "Materials for terahertz science and technology," Nature Materials, Vol. 1, pp. 26-33, Sep., 2002.

[2] Tonouchi, M. "Cutting-edge terahertz technology," Nature Photon., Vol.1, pp. 97-105, Feb., 2007.

[3] D.E. Spence, P.N. Kean, and W. Sibbett, "60-fsec pulse generation from a self-mode-locked Ti:sapphire laser," Opt. Lett., Vol.16, pp. 42-44, Jan., 1991.

[4] D. H. Sutter, G. Steinmeyer, L. Gallmann, N. Matuschek, F. Morier-Genoud, U. Keller, V. Scheuer, G. Angelow, and T. Tschudi , "Semiconductor saturable-absorber mirror assisted Kerr-lens mode-locked Ti:sapphire laser producing pulses in the two-cycle regime," Opt. Lett.,   Vol. 24, pp. 631-633, May, 1999.

[5] D.H. Auston, K.P. Cheung, and P.R. Smith, "Picosecond photoconducting hertzian dipoles," App. Phys. Lett., Vol. 53, pp. 284-286, May, 1984.

[6] X.-C. Zhang, Y. Jin, and X.F. Ma, "Coherent measurement of THz optical rectification from electro-optic crystals," Appl. Phys. Lett., Vol.61, pp. 2764-2766, Sep., 1992.

[7] A. Rice, Y. Jin, X.F. Ma, X.-C. Zhang, D. Bliss, J. Larkin, and M. Alexander, "Terahertz optical rectification from <110> zinc-blende crystals," Appl. Phys. Lett., Vol. 64, pp. 1324-1326, Mar., 1994.

[8] X.-C. Zhang and D.H. Auston, "Optoelectronic measurement of semiconductor surface and interface with femtosecond optics," J. Appl. Phys., Vol. 71, pp. 326-338, Jan., 1991.

[9] Cing-Jung Chuang, "Femtosecond Pulse Shaping Methodology and its Applications in Tera-Hertz radiation enhancement", Master Thesis, Dep. Photonics and Inst. Electro-optical and Eng., National Chiao Tung University, 2004.

[10] Sung-Hui Lin, "The Study of Terahertz Radiation Mechanism from Photoconductive Antenna by Femtosecond Pulse Shaping Technology," Master Thesis, Dep. Photonics and Inst. Electro-optical and Eng., National Chiao Tung University, 2008.

Chapter 2 Principles and Configuration of the Experimental Apparatus

In this chapter, we will introduce the basic theory of pulse shaping and principles of THz pulses generation and detection.

2.1 Theory of Pulse Shaping

What is pulse shaping ?

In a loose definition, it means anything that can change the temporal profile of pulse, but, how to do that ? There are two approaches can be used to modulation the pulses, one is direct modulation the pulses in time. Nanosecond and picoseconds laser pulses can be directly modulation by electronic derived devices [1].

$$E_{out}(t) = h(t) \otimes E_{in}(t) \tag{2.1}$$

On a femtosecond time scale, this method is not suitable due to the limitation of modulation speed of electronic devices. The other approach is modulation the pulses in frequency domain.

$$E_{out}(\omega) = \tilde{H}(\omega) E_{in}(\omega) \tag{2.2}$$

Where $E_{in}(\omega) = F\{E_{in}(t)\}$ is the spectrum of the input pulse, $E_{out}(\omega) = F\{E_{out}(\omega)\}$ is the spectrum of the modulated pulse and $\tilde{H}(\omega)$ is the frequency response. This approach is the so-called "Fourier synthesis method", it was first accomplished by Heritage and Weiner [2], and it's also the mainstream of ultrafast pulse shaping method currently. Figure 2-1 depicts the concepts of pulse shaping in time domain and frequency domain.

(a) Modulation in the time domain

$$E_{in}(t) \longrightarrow \boxed{h(t)} \longrightarrow E_{out}(t) = h(t) \otimes E_{in}(t)$$

$$= \int_{-\infty}^{\infty} h(t-\tau) E(\tau) d\tau$$
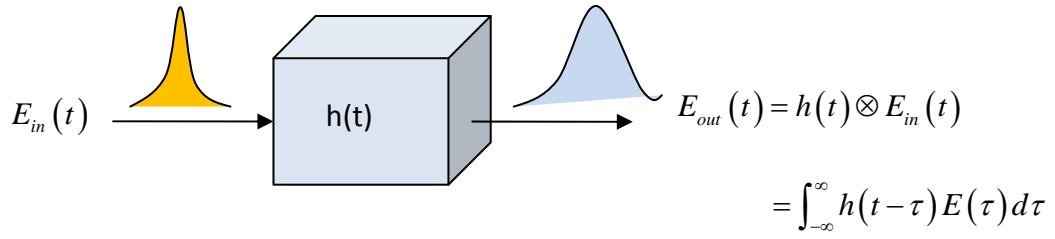
(b) Modulation in the frequency domain

$$E_{in}(\omega) \longrightarrow \boxed{H(\omega)} \longrightarrow E_{out}(\omega) = \tilde{H}(\omega) E_{in}(\omega)$$

$$E_{out}(t) = F^{-1}\{E_{out}(\omega)\}$$
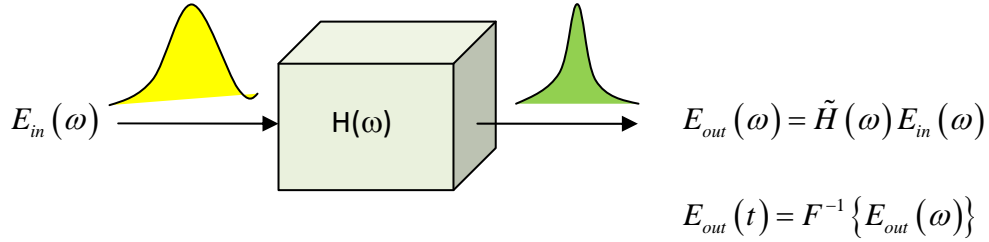
Figure 2-1 Schematic of pulse shaping in (a) time domain (b) frequency domain.

In the approach of Fourier synthesis method, the modulation function we applied is

$$\tilde{H}(\omega) = H_0(\omega) e^{j\phi(\omega)} \tag{2.3}$$

It contains two parts : (1) $H_0(\omega)$ is the amplitude modulation, and (2) $e^{j\phi(\omega)}$ is the phase modulation, conventional modulation devices can be used for pulse shaping include liquid-crystal spatial light modulators [3], acoustic optic modulators [4] and deformable mirrors [5]. In our experiment, we will use LC-SLM as our modulation device, the details are described below.

2.1.1 Measurement of Ultrafast Laser Characteristics

The laser system we used in experiments is a mode-locked Ti-sapphire laser (Tsunami, Spectra-Physics) with a typical output power of 450mW and pulse repetition rate ~82MHz. Figure 2-2 shows the spectrum of our laser source, the FWHM spectra bandwidth is about 40nm.
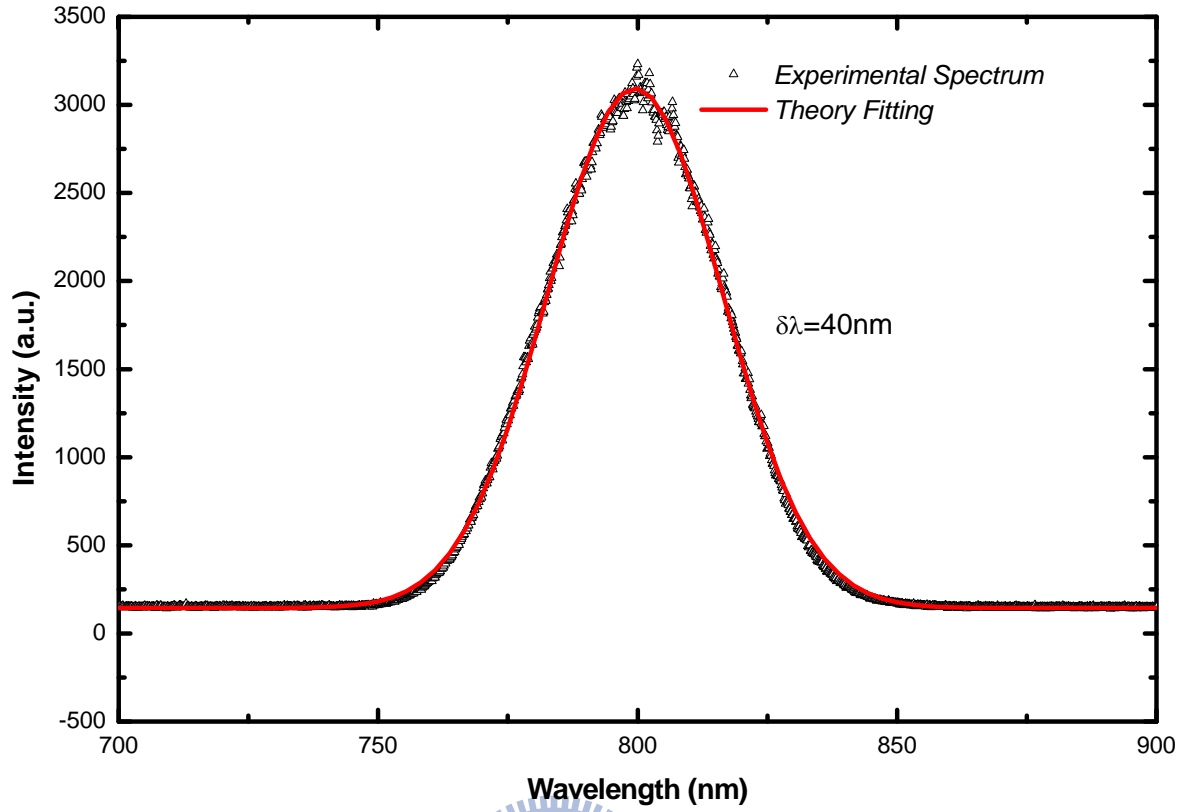
Figure 2-2 Spectrum of the mode-locked Ti-sapphire laser.

According to the Fourier theory, the pulse field in the time domain is the inverse Fourier transform of the frequency domain field :

$$\widetilde{E}(t) = \frac{1}{2\pi} \int_{-\infty}^{\infty} \widetilde{E}(\omega) \exp(i\omega t) d\omega \qquad (2.4)$$

The pulse field in the frequency domain can be written as :

$$\widetilde{E}(\omega) = \sqrt{S(\omega)} \exp\left[j\varphi(\omega) \right] \qquad (2.5)$$

Where $S(\omega)$ is the spectrum and $\varphi(\omega)$ is the spectral phase. We can use this method to estimate the ideal pulse width direct from the measured spectrum :

$$\Delta t_{FWHM} = \frac{2\lambda_0^2 \ln 2}{\pi c \Delta\lambda} \qquad (2.6)$$

Where λ_0 is the central wavelength of laser, $\Delta\lambda$ is the FWHM spectra bandwidth, c is the speed of light. According to equation (2.6), we can know that the ideal pulse width of our laser pulses is about 23.7 fs, it's also called the Transform-Limited Pulse (TLP) width.

In order to understand more information about the pulse, we must measure the temporal profile of the pulse, however, due to the measurement limitation of electronic devices, we cannot direct measure the ultrafast laser pulses in time. The only way we can use to measure the ultrafast pulses is use the pulse to measure itself [6], it's called autocorrelation.

There are several kinds of autocorrelation methods, according to the correlation process we used, autocorrelation can be divided into two classes : (1) Interferometric autocorrelation (2) Intensity autocorrelation. For a complex electric field $\widetilde{E}(t)$, the field autocorrelation is defined by

$$A^{(1)}(\tau) = \int_{-\infty}^{\infty} \widetilde{E}(t)\widetilde{E}(t-\tau)dt \tag{2.7}$$

Figure 2-3 depicts a experiment setup of intensity autocorrelator using second-harmonic generation. A pulse is divided into two, one is variable delayed with respect to the other, and the two pulses are overlapped into a nonlinear medium, such as second-harmonic-generation (SHG) crystal (BBO or LBO) or third-harmonic-generation (THG) crystal. The SHG intensity will be measured vs. delay, yielding the autocorrelation trace.

$$A^{(2)}(\tau) = \int_{-\infty}^{\infty} I(t)I(t-\tau)dt \tag{2.8}$$

Where $I(t) = \left|\widetilde{E}(t)\right|^2$ is the intensity profile of the complex electric field. Figure 2-4 shows the experimental result of intensity autocorrelation.
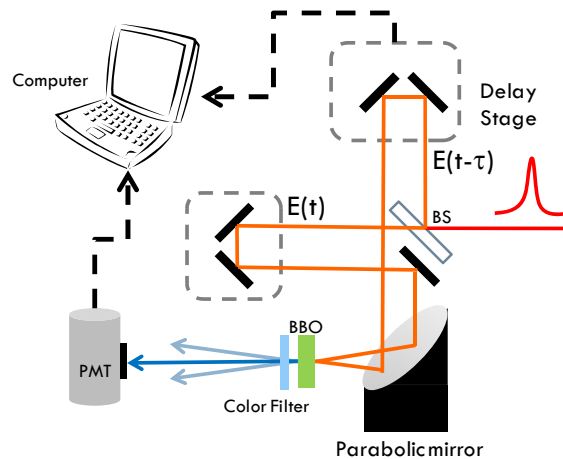
Figure 2-3 Experimental layout for an intensity autocorrelator.

9
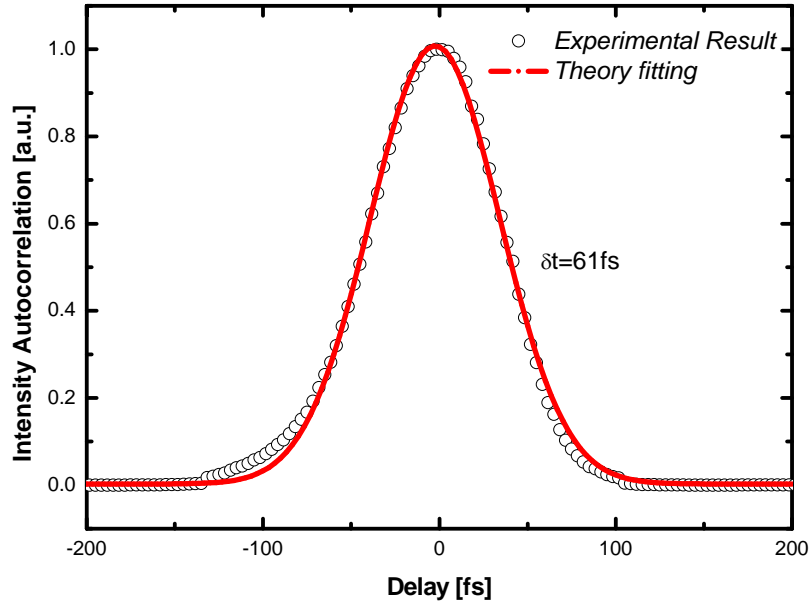
Figure 2-4 Experimental result of the intensity autocorrelation trace.

From the experiment result, we can know that the intensity FWHM pulse width is about 61fs, the TL-pulse width is about 21fs. This difference is due to the 2nd order spectra phase, which will broaden the temporal profile of the pulse. A Gaussian type frequency domain field with spectral phase can be written as :

$$\widetilde{E}(\omega) = E_0 \exp\left[-\left(\frac{\omega - \omega_0}{\Delta\omega}\right)^2\right] \exp\left[j\left(b_0 + \frac{b_1}{2\pi}\omega + \frac{b_2}{4\pi^2}\omega^2 + ...\right)\right] \qquad (2.9)$$

Where b_n is the nth order spectra phase, we only consider the 2nd order phase b_2 in the following discussion, because b_0 wouldn't change the temporal profile of the pulse, and according to the Fourier theory, the 1st order phase b_1 in frequency domain will only cause a linear shift in time, the shape of the pulse also remains the same. The temporal electric field is :

$$\widetilde{E}(t) = F^{-1}\left\{\widetilde{E}(\omega)\right\} \sim E_0 \exp\left[-\frac{t^2/\Delta\omega^2}{4\left(b_2^2 + \frac{1}{\Delta\omega^4}\right)}\right] \exp\left[-j\frac{b_2 t^2}{4\left(b_2^2 + \frac{1}{\Delta\omega^4}\right)}\right] \exp\left[-j\omega_0 t\right] \qquad (2.10)$$

10

From the equation above, we can know that if there exist 2nd order spectra phase b_2, it will causes two effects : (1) Broaden the temporal pulse duration (2) Instantaneous frequency will change with time, it depend on the sign of b_2. If b_2 is greater than zero, the carrier frequency will increase with time, we will say the pulse is *up-chirped* (or positive chirp).

(a) Up-chirped pulse   *(b) Down-chirped pulse*
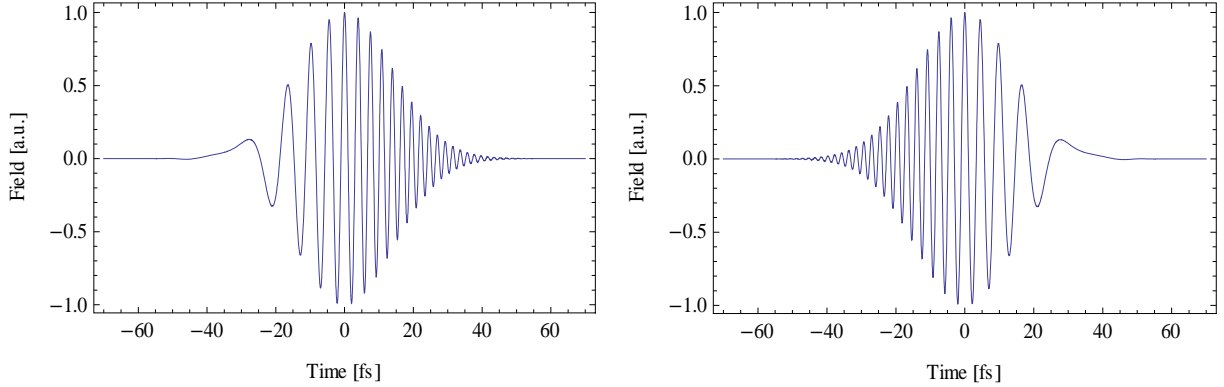
Figure 2-5 (a) An example of up-chirped pulse, it means the instantaneous frequency is increase with time. (b) down-chirped pulse, the instantaneous frequency is decrease with time.

The relationship between 2nd order spectra phase b_2 and temporal pulse width w is :

$$w = \tau_0 \sqrt{1 + \left(\frac{4 \ln 2 \frac{b_2}{2\pi^2}}{\tau_0^2} \right)^2} \tag{2.11}$$

where τ_0 is the transform-limited pulse width.

From equation(2.11) we can know that, if two pulses with the same 2nd order spectra phase b_2, they will have the same pulse width, however, the physical meaning are quite different. A pulse is called positive-chirped if lower frequency light travels ahead of higher frequency light and negative if opposite holds.

We will discuss the role of chirp in the processes of THz pulses excitation and detection in the next chapter.

2.1.2 Pulse Measurement in Time-Frequency Domain

Although autocorrelation is a convenient method to measure the temporal profile of the pulses, however, the phase of the pulse is an unsolvable problem, in many applications of ultrafast laser, the phase of the pulse plays very important role. In additional, there exist ambiguities of the temporal shape, two different temporal profile may lead to the same autocorrelation trace.

*F*requency-*R*esolved-*O*ptical-*G*ating (FROG) [7] is developed to measure the amplitude and phase of the ultrafast laser pulse. The basic concept of FROG is similar to autocorrelation, it measures spectrum of the correlation signal vs. delay :

$$I_{FROG}(\tau,\omega) = \int_{-\infty}^{\infty} P(t)G(t-\tau)e^{-j\omega t}dt \tag{2.12}$$

Where $P(t)$ is the complex electric field we want to measure, $G(t)$ is the gating function, it depends on what kind of nonlinear process we used, and will have different forms. After measuring FROG trace, an iterative method is used to reconstruct the original complex pulse. And then we can get the information of the pulse amplitude and phase. Figure 2-6 shows an example of FROG trace.
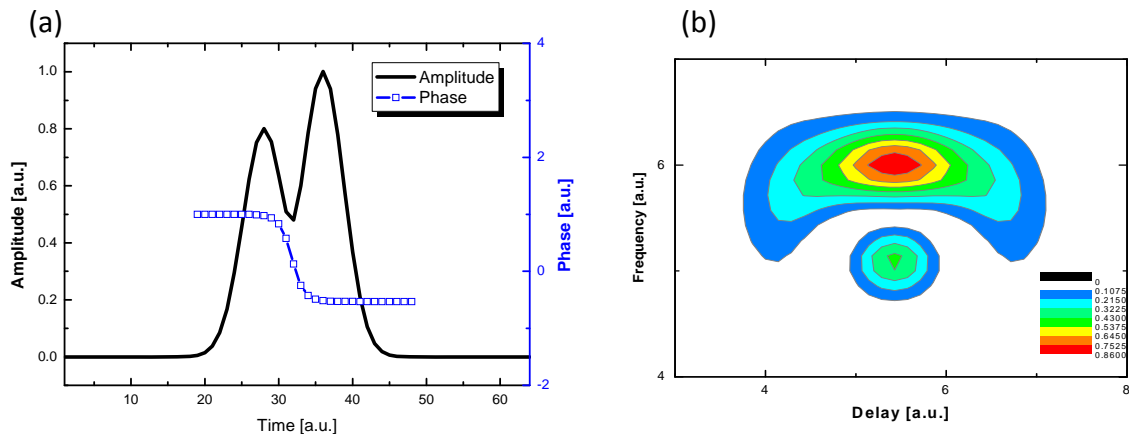
Figure 2-6 An example of SHG-FROG trace [8], (a) amplitude and phase of the pulse in time-domain, and (b) the corresponding SHG-FROG trace.

12

2.1.3 Dispersion Free Pulse Shaping System

Figure 2-7 depicts the dispersion free pulse shaping system, this system consists of a pair of gratings (600 grooves/mm), two spherical reflectors with a focal length f=20cm and two reflection mirrors. Optical pulse will be diffracted by first grating and then focus by the spherical reflector, the first two components performs a Fourier transform which converts the angular dispersion from the grating to a spatial separation. LC-SLM is placed in the Frequency domain in order to manipulate the spatially dispersed optical Fourier components. After a second spherical reflector and grating recombine all the frequencies into a single collimated beam, a shaped output pulse is obtained.

Optical pulse shaping is accomplished utilizing a programmable spatial light modulator [9] (SLM Cambridge Research and Instrumentation Inc. (CRI) Woburn, MA, SLM-128). The SLM which induce a individual phase retardation on the pulse spectrum consists of 128 pixels, each pixel with 5 mm high and 100 μm width. We can tailor and design different pulse waveforms using GS algorithm [10].
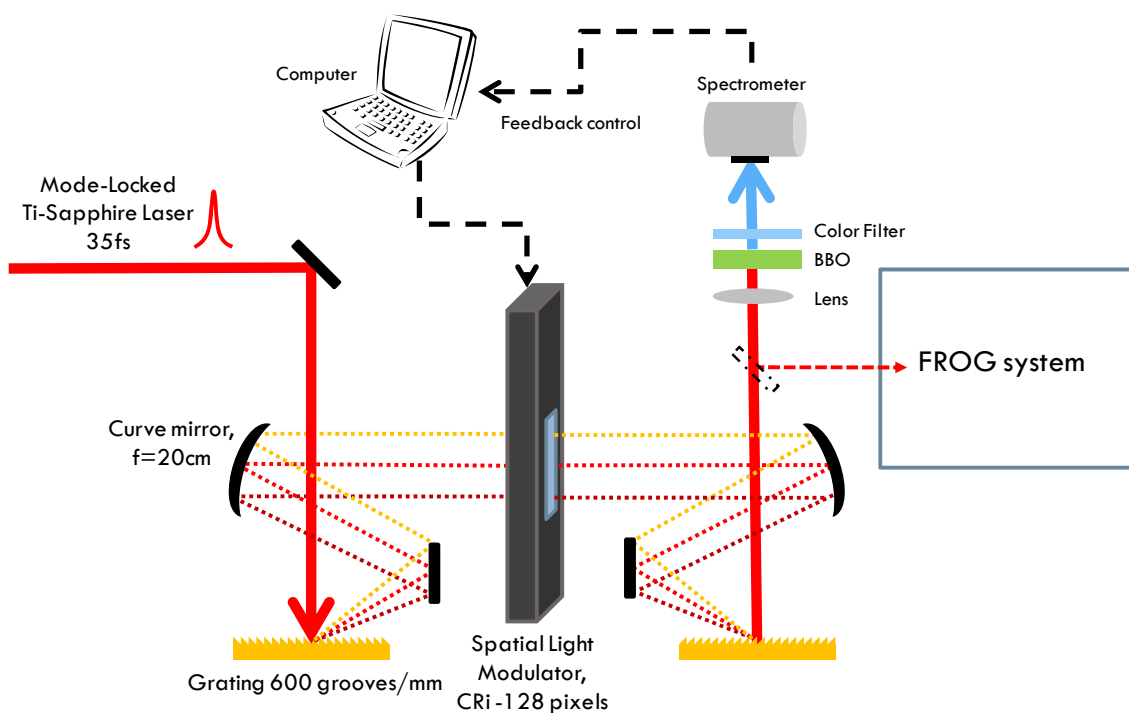
Figure 2-7 Schematic of dispersion-free pulse shaping system.

2.1.4 Freezing Phase Algorithm

In the previous discussion, we know that if there exist 2nd order spectra phase b$_2$, it will broaden the temporal profile of the pulse, and induce linear chirp. If we can compensate this phase in frequency domain, then we can get transform-limited pulse with shorter pulse duration and higher peak intensity than the chirped pulse.

Traditional phase compensation algorithms including simulated annealing algorithm [11], and genetic algorithm [12], we adopt freezing phase algorithm [13] to compensate the spectra phase, which is very rapid compare with other algorithms. The concept of freezing phase algorithm (FPA) is illustrated below.

The mode-locked pulse can be expanded by its spectra components in frequency domain :

$$\widetilde{E}(t) = \sum_{n=1}^{N} A_n \exp\left[j\left(\omega_n t + \phi_n\right)\right] \exp\left[j\theta_0\right]$$
$$= \sum_{n=1}^{N} A_n \exp\left[j\left(\left(\omega_0 + n\Delta\omega\right)t + \phi_n\right)\right] \exp\left[j\theta_0\right] \tag{2.13}$$

Where A_n, ϕ_n and ω_n represent the amplitude, phase and its carrier frequency respectively, all this phase compensation algorithms are attempt to compensate the spectra phase ϕ_n.

Figure 2-7 depicts the experiment apparatus of freezing phase algorithm, the laser pulse is expanded into frequency domain, each frequency components will be turning by SLM, after recombination by the 2nd grating, the laser pulse is focused by a lens into a nonlinear crystal (type-I BBO), the SHG signal will be measured by a spectrometer, the total power of the pulses will be return to computer as feedback control.

We can use phasor to represent each spectra phase components $v_n = \exp\left[j\phi_n\right]$, here we only use 3 phasors $v_1 \sim v_3$ to simplify the freezing process. Figure 2-8 (b) show the transformation process of each phasors during freezing phase algorithm. First we pick up one of the phasors v_3 and make the other phasors v_1 and v_2 as one group, then turning v_3 from 0~2π by SLM, during the turning process, we measuring the power of the SHG signal. If

v_3 are in the same direction of $v_1 + v_2$, it will have maximum SHG intensity, we can use this concept to determine the spectra phase of that component. Second, we pick another phasor v_2 and regroup the other SLM pixels, then determine the phase of v_2. Finally, all the spectra phase will be compensated after freezing, figure 2-8(a) shows the flowchart of freezing phase algorithm.

(a)   (b)
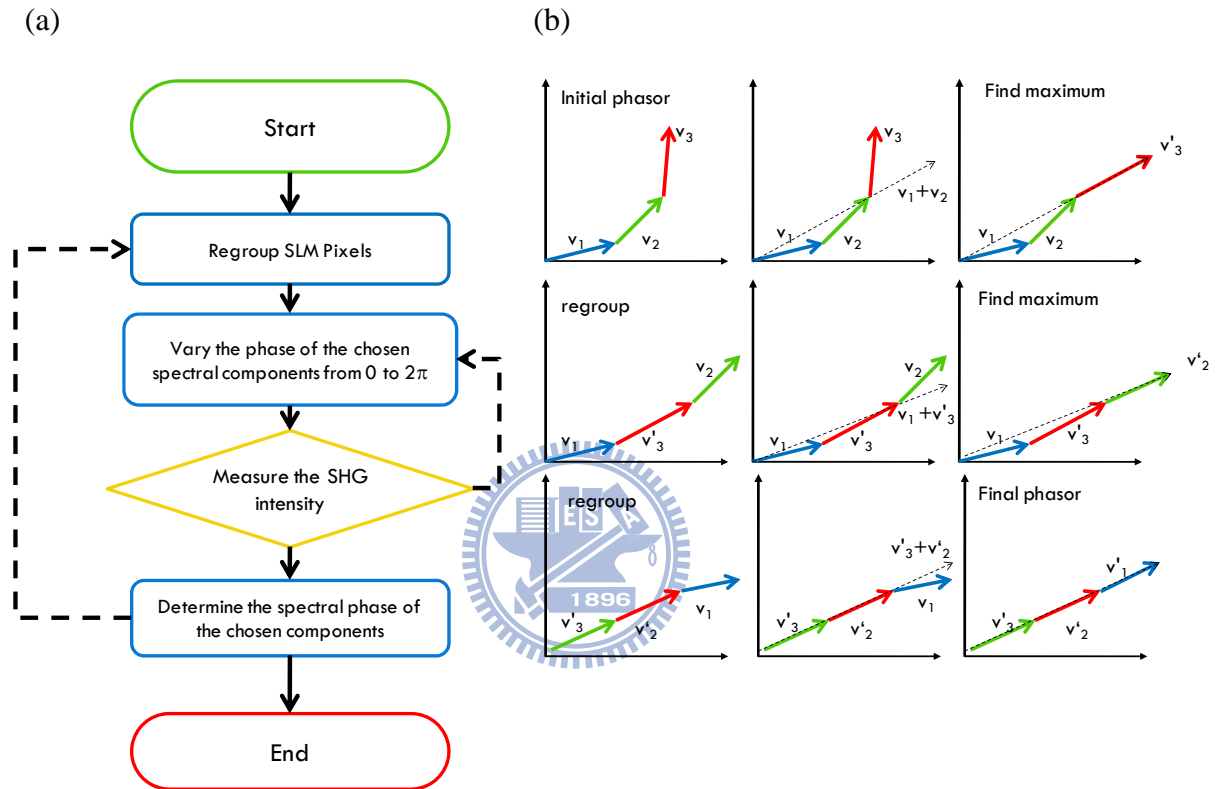
Figure 2-8 (a) Flow chart of Freezing Phase Algorithm (b) Schematic of the freezing process.

Figure 2-9 (a) shows the autocorrelation trace of the laser pulse, we can see that the pulse width is about 100fs before freezing procedure. After freezing phase, the pulse width is about 38fs. The compensated phase of SLM is shown in Figure 2-9 (b).
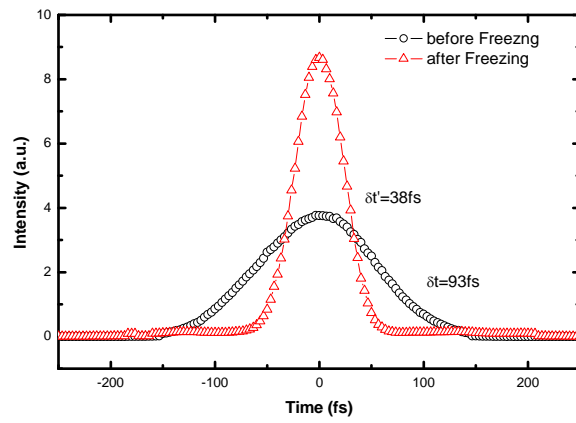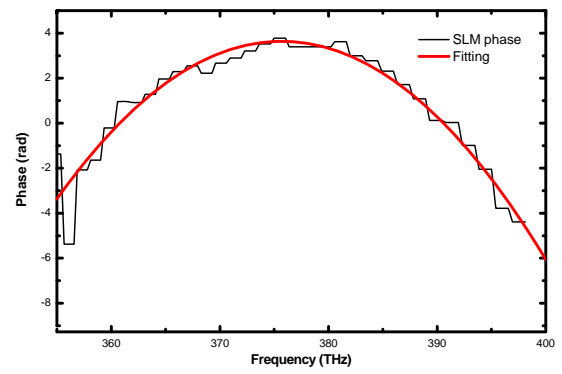
Figure 2-9 (a) autocorrelation trace of the pulse : circle - before freezing phase procedure, triangle – after freezing phase procedure, and (b) the compensated phase in the SLM.
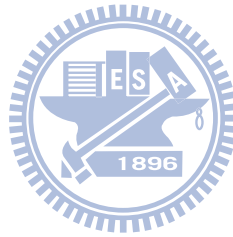
2.2 Terahertz-Pulse Generation from Photoconductive Antenna
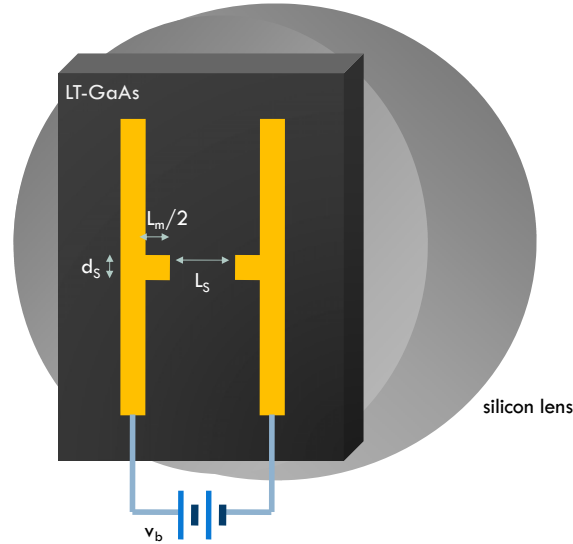
Figure 2-10 Schematic view of photoconductive dipole antenna.

The schematic view of photoconductive antenna we used in experiment is shown in Figure 2-10, the antenna with dipole structure is fabricated on low-temperature grown (LT) GaAs, which has very high breakdown field and fast carrier life time (~ps) along with good mobility (~200 $cm^2V^{-1}s^{-1}$). The LT-GaAs substrate is attached with a silicon lens, which is used to efficiently coupling the THz radiation out of the LT-GaAs substrate.

When the photoconductive gap is irradiated by femtosecond laser pulses with energy greater than the band gap of the semiconductor, electrons and holes pairs are generated in the conduction band and valance band respectively. The carriers are then accelerated by the bias field and decay with a time constant τ_C, resulting in a pulsed photocurrent $J(t)$ in the photoconductive antenna, this transient current will induce electromagnetic transient (THz radiation), the radiated electric field is proportional to the first-order time derivate of the transient current :

$$E_{THz}(t) \propto \frac{\partial J(t)}{\partial t} \tag{2.14}$$

2.2.1 One Dimensional Drude-Lorentz Model

In order to understand the carrier transport mechanism in the THz radiation generation process, one dimensional Drude-Lorentz model [14-16] is used in this study. When the biased semiconductor is irradiated by the femtosecond laser pulses with energy greater than its bandgap, the electron-hole pairs are generated, the time dependence of the carrier density $n(t)$ is :

$$\frac{dn(t)}{dt} = -\frac{n(t)}{\tau_c} + G(t) \tag{2.15}$$

Where τ_c is the carrier trapping time, and $G(t)$ is the generation rate of the carrier by the laser pulse, assume the generation rate of the carrier is direct proportional to the laser pulse, it can be written as

$$G(t) = n_0 \exp\left[-\left(\frac{t}{t_p/2\sqrt{\ln 2}}\right)^2\right] \tag{2.16}$$

Where n_0 represents the carrier generation density at t=0 ps, t_p is the intensity FWHM of the laser pulse. The generated carriers will be accelerated in the bias electric field, the acceleration of electrons and holes is given by

$$\frac{dv_{e,h}(t)}{dt} = -\frac{v_e(t)}{\tau_s} + \frac{q_{e,h}}{m_{e,h}} E(t) \tag{2.17}$$

Where $v_{e,h}(t)$ is the average velocity of the carrier, $q_{e,h}$ is the charge of an electron (hole), τ_s is the momentum relaxation time, $m_{e,h}$ is the effective mass of the electron (hole), and $E(t)$ is the local electric field.

The local electric field $E(t)$ is smaller than the applied bias field, E_{bias}, due to the

screening effects[17] of the space charge,

$$E(t) = E_{bias} - \frac{P(t)}{\alpha\varepsilon} \tag{2.18}$$

Where $P(t)$ is the polarization induced by the spatial separation of the electron and hole, ε is dielectric constant of the substrate, and α is the geometrical factor of the semiconductor [18]. The time dependence of polarization $P(t)$ can be written as

$$\frac{dP(t)}{dt} = -\frac{P(t)}{\tau_r} + J(t) \tag{2.19}$$

Where τ_r is the recombination time between an electron and hole, $J(t)$ is the current density contributed by an electron and hole,

$$J(t) = en(t)\left[v_h(t) - v_e(t)\right] = en(t)v(t) \tag{2.20}$$

Where e is the charge of a proton, and the change of electric currents leads to electromagnetic radiation according to Maxwell's equations. The far field of the radiation $E_{THz}(t)$ is given by

$$E_{THz}(t) \propto \frac{dJ(t)}{dt} = ev(t)\frac{dn(t)}{dt} + en(t)\frac{dv(t)}{dt} \tag{2.21}$$

In the following section, we will show the simulation results of THz radiation generation from the Drude-Lorentz model of photoconductive antenna.

2.2.2 Simulation Results and Discussion

The coupled differential equations (2.15)-(2.20) can be numerically solved by fourth order Runge-Kutta method [19], the parameters we used in the simulation are listed in Table 2-1.

Table 2-1 Parameters used in the THz radiation generation simulation

parameters		parameters	
Carrier life time τ_c	0.5 [ps]	Carrier density n_0	10^{24} [m^{-3}]
Momentum relaxation time τ_s	0.2 [ps]	Effective mass of electron m_e	0.067 m_0
Recombination time τ_r	10 [ps]	Effective mass of hole m_h	0.37 m_0
Pulse duration t_p	100 [fs]	Applied bias field E_{bias}	10^6 [V/m]
Charge of electron q_e	1.6*10^{-19} [Q]	Geometrical factor α	900
Charge of electron q_h	1.6*10^{-19} [Q]	Relative Static Permittivity ε_r	12.96

From the 1D Drude-Lorentz model, we can know that there are several factors will influence the THz generation, such as A. Excitation pulse width t_p, B. Carrier life/trapping time τ_c, C. Momentum relaxation time τ_s, D. Bias field E_b, and E. Excitation density n_0. We will show the simulation results and discuss its impact below.

A. Excitation pulse width dependence

(a) Time Domain   (b) Power Spectrum
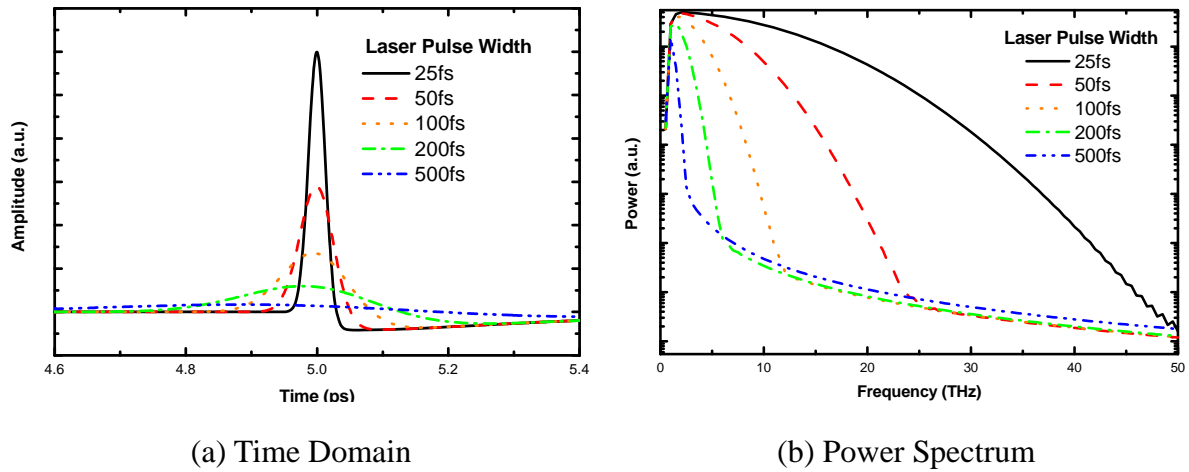
Figure 2-11 Simulated THz field at excitation pulse width t_p of 25fs, 50fs, 100fs, 200fs, and

500fs, (a) time domain profile and (b) power spectrum.
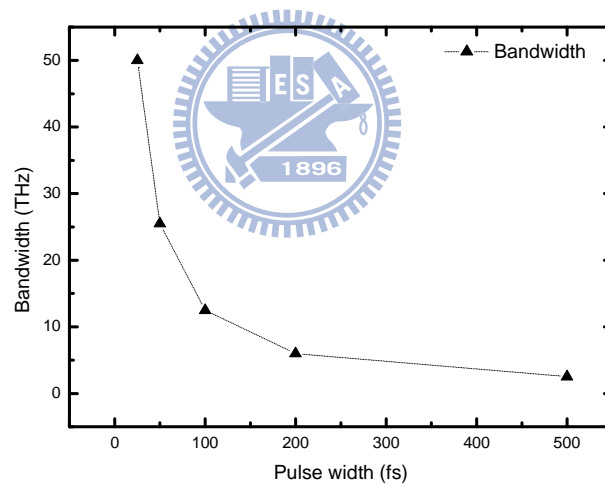
Figure 2-12 Excitation pulse width dependence of THz bandwidth.

Figure 2-11 shows (a) the simulated THz pulses generated from different excitation pulse

width, and (b) the corresponding power spectrum. From the simulation results we can know

that the more shorter excitation pulse width, the broader bandwidth and higher power THz

pulse we can get, the relationship between excitation pulse width and efficient THz bandwidth

is shown in Figure 2-12.

B. Carrier life time/trapping time dependence

(a) Time Domain
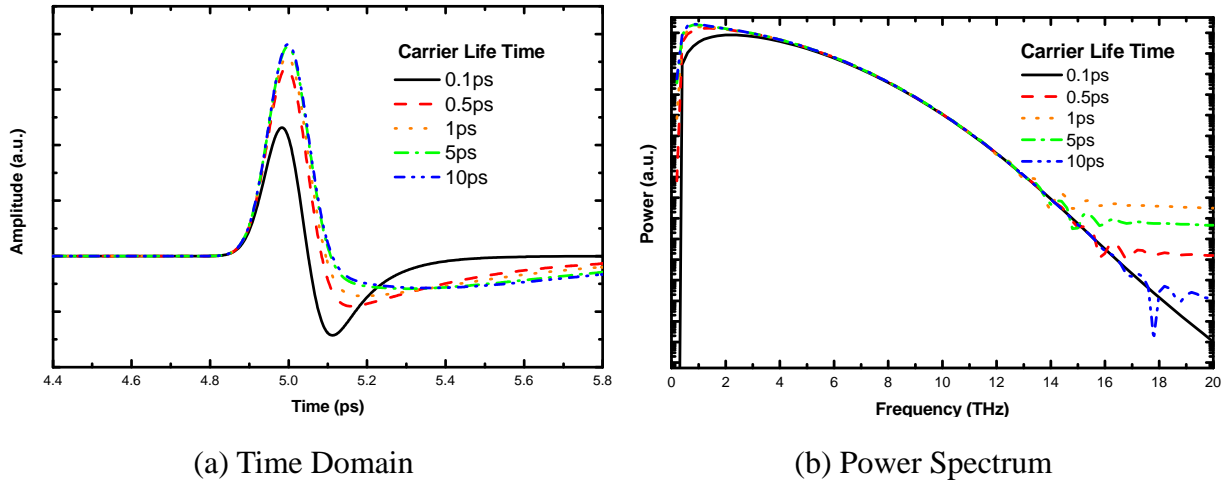
(b) Power Spectrum

Figure 2-13 Simulated THz field at carrier life time τ_c of 0.1ps, 0.5ps, 1ps, 5ps, and 10ps, (a) time domain profile and (b) power spectrum.

(a)

(b)
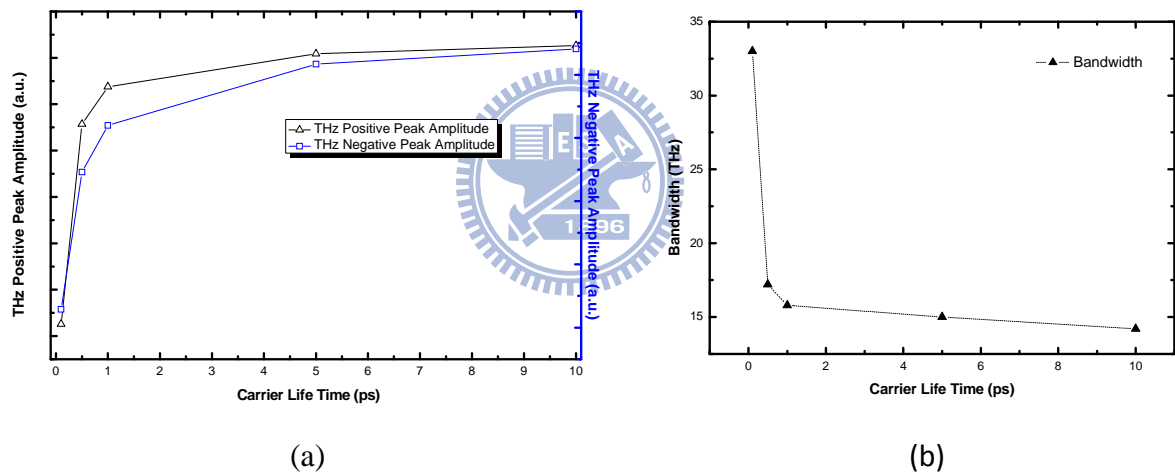
Figure 2-14 Relationship between carrier life time and (a) THz positive & negative amplitude (b) bandwidth.

Figure 2-13 shows (a) the simulated THz pulses generated with different carrier life time, and (b) the corresponding power spectrum. From the simulation results we can know that the faster the carrier life time, the broader bandwidth we can get, however, it will sacrifice the total power of THz radiation. From figure 2-14, we can know that suitable carrier life time will have both higher THz radiation power and broader bandwidth.
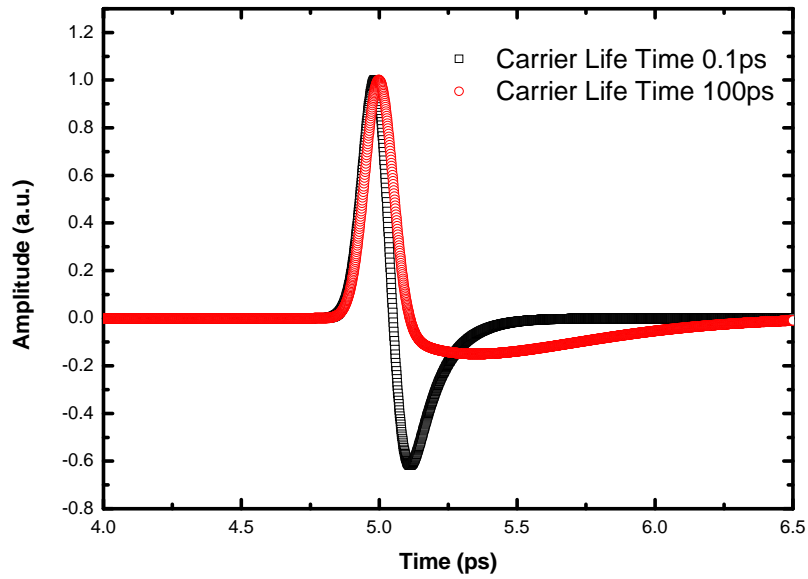
Figure 2-15 Comparison of THz waveforms generated with shorter and longer carrier time,

the peak value is normalized to 1 respectively.

From Figure 2-15, we can compare the two different waveforms calculated with shorter

carrier life time (0.1ps) and longer carrier life time(100ps), it shows two different kinds

waveform – bipolar waveform(0.1ps) and unipolar(100ps) waveform, it's agree with the

experiment results [21].

C. Momentum relaxation time dependence

(a) Time Domain
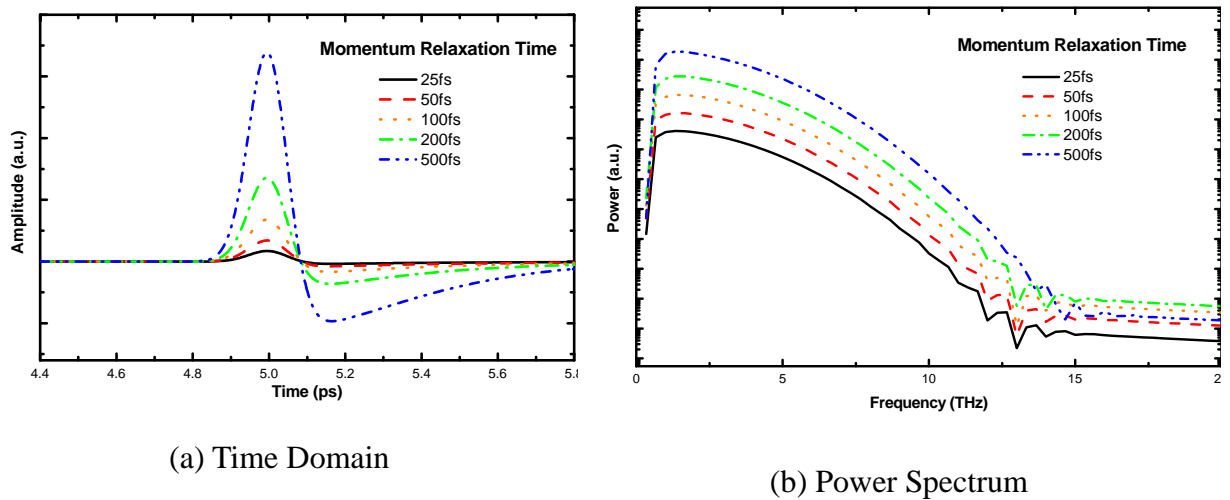
(b) Power Spectrum

Figure 2-16 Simulated THz field at momentum relaxation time τ_s of 25fs, 50fs, 100fs, 200fs,

and 500fs, (a) time domain profile and (b) power spectrum.

The momentum relaxation time it's also very important in the THz field generation process, from Figure 2-16, we can find out the amplitude of THz radiation increases as the momentum relaxation time increases. The momentum relaxation time is corresponding to the saturation velocity of the carriers, the higher the saturation velocity, the higher THz peak amplitude we can get.

D. Bias Field Dependence

(a) Time Domain   (b) Power Spectrum
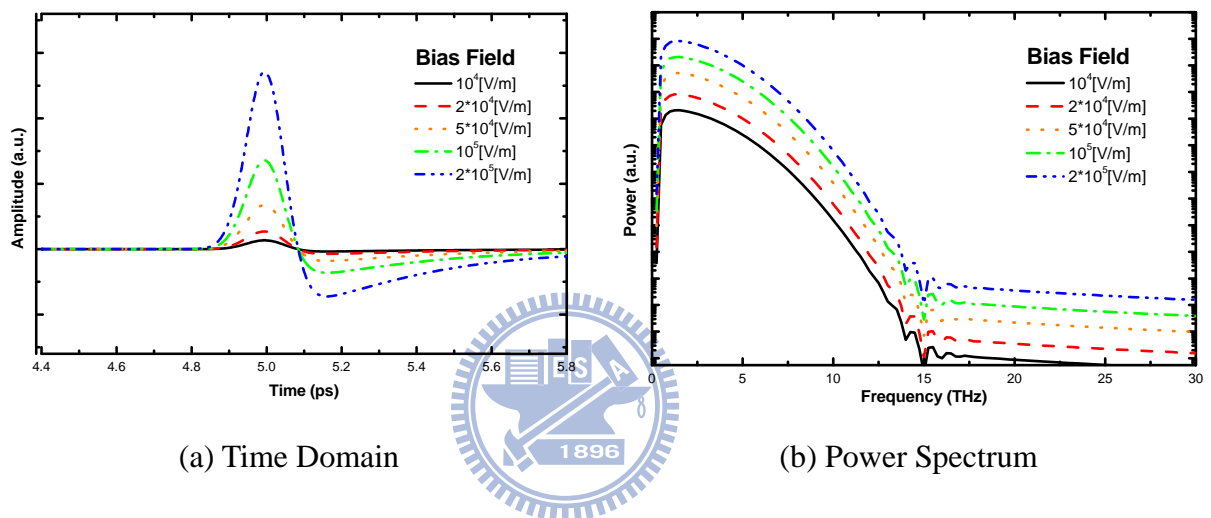
Figure 2-17 Simulated THz field at bias field E_b of 10^4 [V/m], 2×10^4 [V/m], 5×10^4 [V/m], 10^5 [V/m], and 2×10^5 [V/m] (a) time domain profile and (b) power spectrum.

The bias electric field provides the acceleration of electrons and holes, when we increase bias field, it can also increase the saturation velocity, so we can get higher peak amplitude of THz field, however, the efficient bandwidth is remains unchanged under higher bias field.

E. Excitation density dependence

(a) Time Domain   (b) Power Spectrum
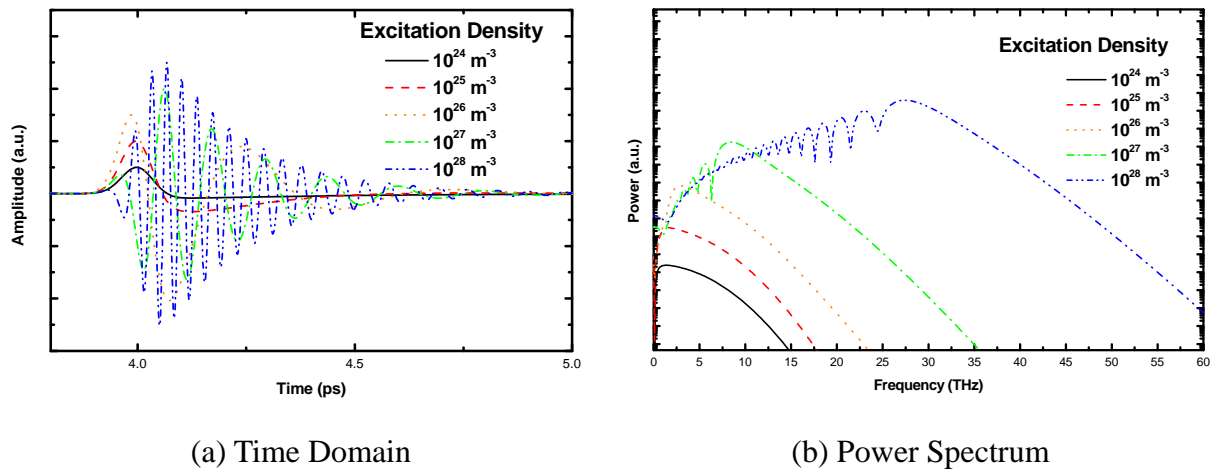
Figure 2-18 Simulated THz field at excitation density n_0 of 10^{24} [m^{-3}], 10^{25} [m^{-3}], 5×10^{26} [m^{-3}], 10^{27} [m^{-3}], and 10^{28} [m^{-3}] (a) time domain profile and (b) power spectrum.

When the electrons and holes are generated by the optical pulses, it will be accelerated in opposite directions in the local electric field. This induces a polarization, which acts as a restoring force for the motion of electrons and holes, when the carrier density increase, the local electric field can be screened to a comparable magnitude of the restoring force. In that case, the electrons and holes will serves as an oscillator, and induces an oscillation electric field. From the simulation results in Figure 2-18, it shows different THz fields generated at various carrier densities. We can see the amplitude of the THz field increases and tends to oscillate as the increase of the carrier density. This results shows the possibility to get THz fields with higher frequency using screening effect.

2.3 Terahertz-Pulse Detection with Photoconductive Antenna

The pulse duration of the THz radiated from the PC antenna is typically several picoseconds, in order to obtain the temporal profile of the THz waveform, cross-correlation measurement is used. According to the measurement mechanism, it can be majorly divided into two methods : (1) Electro-Optical sampling [20-21], (2) Photoconductive sampling [15,21]. The principle of PC sampling method is discussed below.

2.3.1 Experiment Setup of THz-Time Domain System

The experimental setup of the photoconductive THz time domain system is shown in Figure 2-19. The optical pulse will be divided into two pulses by a beam splitter, one serves as pump pulse, the other is probe pulse. After excitation the THz antenna by the pump pulse, the emitted THz pulse is collimated and then focused by a pair of off-axis parabolic mirrors on to a PC antenna detector. The PC detector is gated with the probe optical pulse, which will induce the time-dependent conductance, it will convolute with the incident THz field, after delaying the timing of the gate pulse to the pump pulse, the temporal waveform of the THz pulse is obtained.
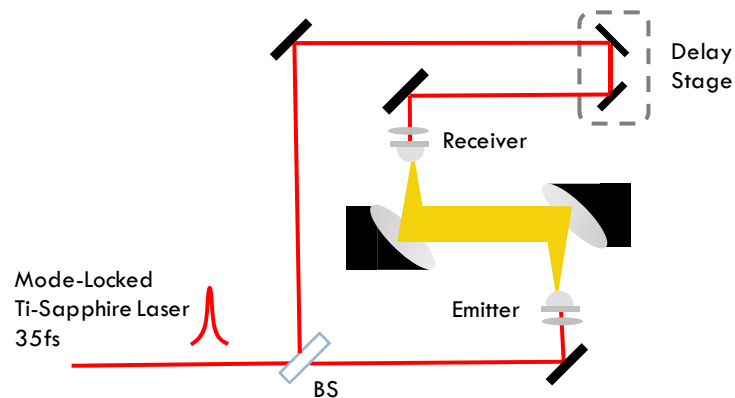
Figure 2-19 Experimental setup of THz-Time Domain System.

2.3.2 Detection Principle

When the photoconductive gap is irradiated with femtosecond optical pulse, the electron-hole pairs are generated, and induce the time-dependent conductance $g(t)$, the incident THz field will induce bias voltage $E_g(t)$ across the photoconductive gap, it will correlated with the time-dependent conductance and induced the photocurrent $I_{PC}(\tau)$:

$$I_{PC}(\tau) \equiv \frac{Q(\tau)}{T} = \int_{-\infty}^{\infty} dt E_g(t) g(t-\tau) \tag{2.22}$$

Where $Q(\tau)$ is the collected charge for each gate pulse, $1/T$ is the repetition rate of the laser. The induced bias voltage $E_g(t)$ across the photoconductive gap is given by

$$E_g(t) = F^{-1}\left\{ E_{THz}(\omega) H_{Antenna}(\omega) \right\} \tag{2.23}$$

Where $E_{THz}(\omega)$ is the Fourier transform of the incoming THz electric field to the antenna, and $H_{Antenna}(\omega)$ is the PC antenna response of the detector, it will be discussed in section 2.3.3. The time-dependent conductance is

$$g(t) = \int^{t} dt' I_g(t') \left(1 - e^{-\frac{(t-t')}{\tau_S}} \right) e^{-\frac{(t-t')}{\tau_C}} \tag{2.24}$$

Where $I_g(t)$ is the temporal intensity profile of the gating pulse, and τ_s is the momentum relaxation time and τ_c is the carrier life time. The first part of the eq. (2.24) is corresponding to the photocurrent rise mechanism, and the second part of eq. (2.24) represents the current recover mechanism, the simulation results of PC sampling is shown in section 2.3.4.

2.3.3 Antenna Response of THz detector

When the THz field is focused on to the PC detector, we must consider the impedance matching conditions between the PC antenna and the transmission line, it could be frequency dependent and results a frequency dependent response function $H_{Antenna}(\omega)$, which will reshape the temporal waveform of the THz pulse, the detail discussion of PC antenna response is reported by Jepsen et al [15], we will just show the conclusions below.

The frequency-dependent photocurrent induced in the photoconduction gap is given by :

$$I(\nu) = \xi P_{laser} \sqrt{\frac{c_0 P_{THz}}{\pi\varepsilon_0}} \frac{2R_L t_s}{L_s^2 dw_0 (n-1)} \frac{1}{\nu} Erf[\frac{L}{2}\frac{(n-1)\pi w_0}{cR_L}]Erf\left[\frac{d}{2}\frac{(n-1)\pi w_0}{cR_L}\right] \qquad (2.25)$$

Where ξ is the conversion factor between laser power and number of photogenerated carriers, P_{laser} is the power of laser, c_0 is the speed of light, P_{THz} is the total power of the THz beam, R_L is total resistance over the detector, t_s is the thickness of the semiconductor layer covering the detection area, and w_0 is initial spot size of the THz beam.

A. Low-frequency limit

In the low-frequency case, the wavelength of the THz field is much longer than any dimension of the detector, the response function simplifies to

$$I_{\nu\to 0}(\nu) = \xi P_{laser} \sqrt{\frac{c_0 P_{THz}}{\pi\varepsilon_0}} \frac{2(n-1)\pi w_0}{c_0^2 R_L} \frac{t_s(L_S + L_M)}{L_S^2} \nu \propto \nu \qquad (2.26)$$

The response increases proportion to the frequency of THz radiation, it results in a signal differentiation in time domain. According to Fourier theory, a multiplication of signal by ν corresponding to a differentiation in the time domain.

$$F^{-1}\{-j\omega G(\omega)\} = \frac{d}{dt}g(t) \qquad (2.27)$$

B. High-frequency limit

In the other hand, for high-frequency case, the wavelength of the THz radiation is much smaller than the detector dimensions, the response function simplifies to

$$I_{\nu \to \infty}(\nu) = \xi P_{laser} \sqrt{\frac{c_0 P_{THz}}{\pi \varepsilon_0}} \frac{2R_L t}{L_s^2 dw_0 (n-1)} \frac{1}{\nu} \propto \frac{1}{\nu} \tag{2.28}$$

The response is inverse proportion to the frequency of THz radiation, it results in a signal integration in time domain. According to Fourier theory, a division of signal by ν corresponding to a integration in the time domain.

$$F^{-1}\left\{\frac{1}{j\omega} G(\omega)\right\} = \int g(t)\, dt \tag{2.29}$$

From the discuss above, we can make a brief conclusion of the antenna response function :

(1) For smaller detector in lower THz range (several THz), the response function of the antenna can be simplify to $\widetilde{H}_{Antenna}(\omega) = j\omega$, which results in a signal differentiation in time domain.

(2) For large detector in higher THz range, the response function of antenna can be simplify to $\widetilde{H}_{Antenna} = \frac{1}{j\omega}$, which results in a integration in time domain.

(3) For finite-sized detector for low frequencies will works as differentiator, and for high frequencies as in integrator in time-domain.

2.3.4 Simulation Results and Discussion

In order to understand the role of carrier life and momentum relaxation time in the sampling process, we consider the time-dependence conductance at two cases : (1) change carrier life time (2) change momentum relaxation time, the simulated results are shown in Figure 2-20 and Figure 2-21 respectively.

(a)   (b)
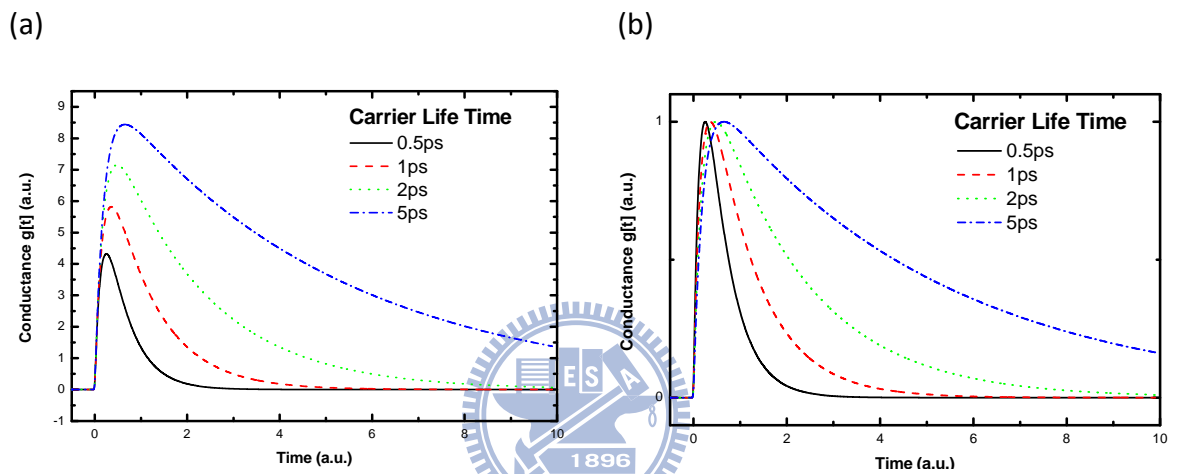
Figure 2-20 (a) Time dependence conductance $g(t)$ at carrier life time τ_c of 0.5ps, 1ps, 2ps, and 5ps, (b) normalize the peak amplitude of (a) to 1.

(a)   (b)
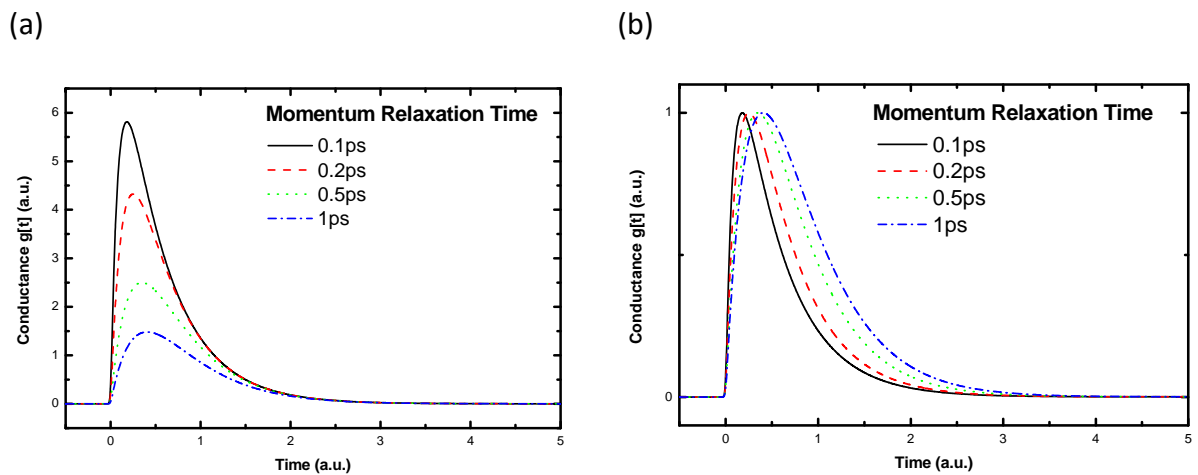
Figure 2-21 (a) Time dependence conductance $g(t)$ at momentum relaxation time τ_s of 0.1ps, 0.2ps, 0.5ps, and 1ps, (b) normalize the peak amplitude of (a) to 1.

From the simulation results above, we can know that if the material with shorter momentum relaxation time, the time dependence conductance will have much higher peak conductance, and results in a much delta-function like shape. For carrier life time, the simulation results show that the material with longer carrier time will have much higher peak conductance, the time duration of the conductance will increase simultaneously, Although the higher conductance will get much higher current in the convolution process, however, the broader time duration will cause "sampling effect", the actual signal will be distorted under longer gating window, it will influence the applications of THz time domain spectroscopy, we will discuss it in chapter 4.
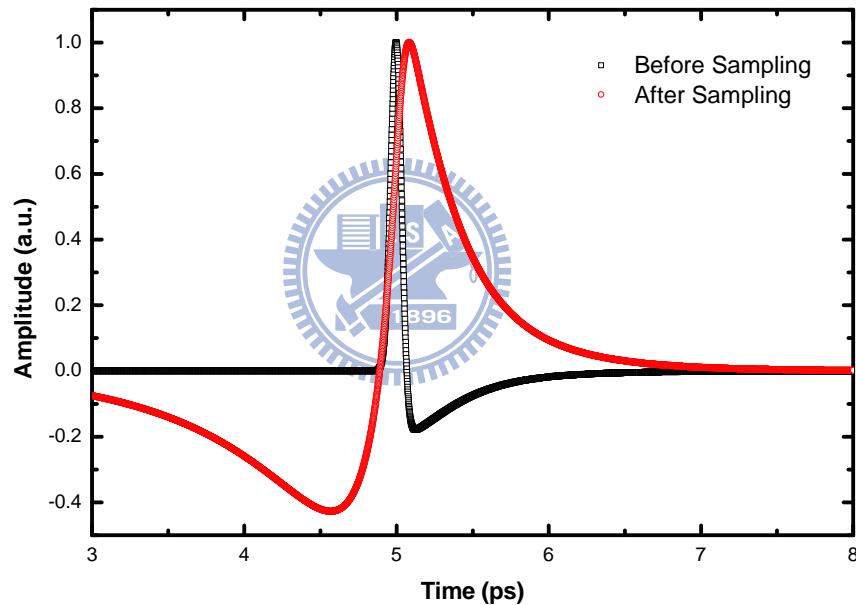
Figure 2-22 Original THz waveform and its sampling waveform by PC antenna(without antenna response).

Figure 2-22 shows the simulated THz electric field and its waveform sampling by PC antenna, we can see that the original THz field is distorted during sampling process. When the time-dependent conductance is convolved with bipolar waveforms, the first half cycle is greatly reduced, while the latter half is less affected, leading to the above observations, the influence of carrier life time and momentum relaxation time in the sampling process is discussed below.

A. Carrier Life Time dependence

The simulated sampling waveform with different carrier life time is shown in Figure 2-23(without antenna response) and Figure 2-24(with antenna response). From the simulation results, we can find out if the material with fast carrier life time, the measured signal will have smaller peak amplitude compare with the slower carrier time material, however, it can preserve the original waveform and get broader bandwidth.
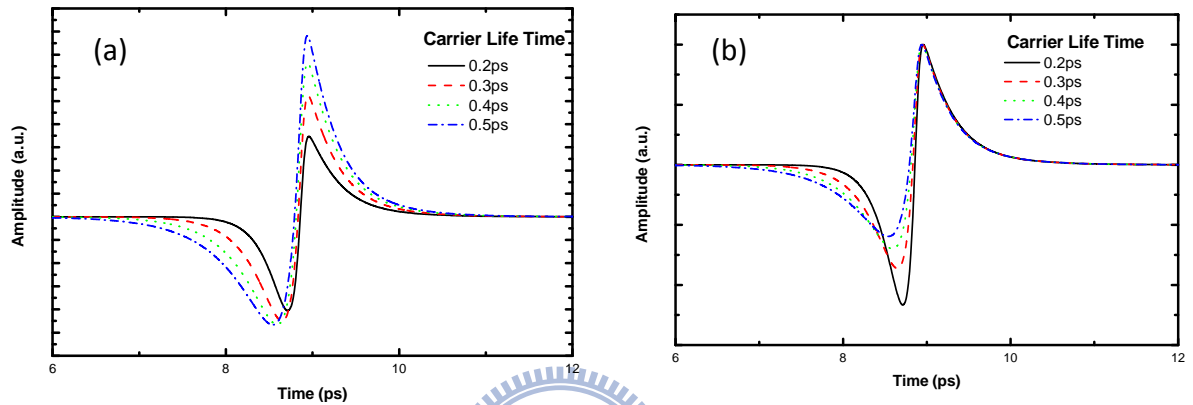
Figure 2-23 (a) Simulated THz fields sampling(without antenna response) with different materials at carrier life time τ_c of 0.2ps, 0.3ps, 0.4ps, and 0.5ps, (b) normalize the peak amplitude of (a) to 1.
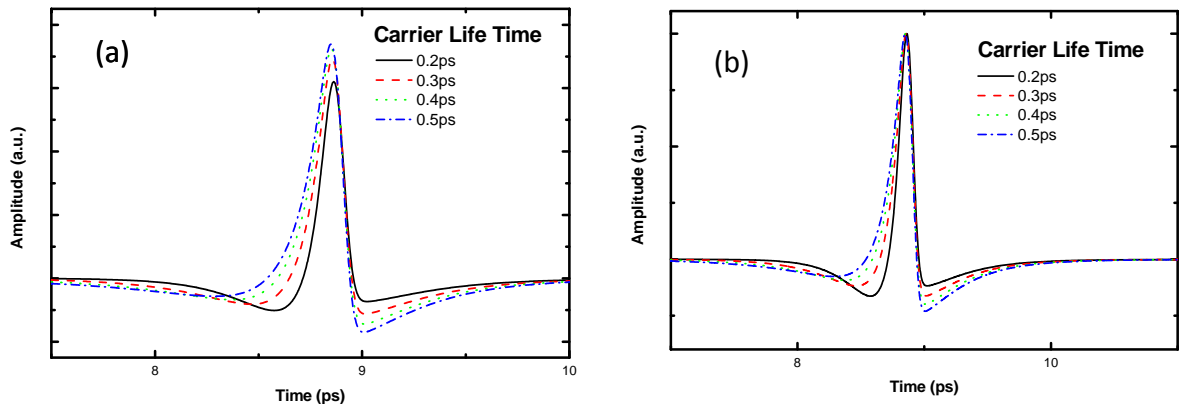
Figure 2-24 (a) Simulated THz fields sampling(with antenna response) with different materials at carrier life time τ_c of 0.2ps, 0.3ps, 0.4ps, and 0.5ps, (b) normalize the peak amplitude of (a) to 1.

B. Momentum Relaxation Time dependence

The simulated sampling waveform with different momentum relaxation time is shown in Figure 2-25(without antenna response) and Figure 2-26(with antenna response). From the simulation results, we can find out if the material with fast momentum relaxation time, the measured signal will have higher peak amplitude and broader bandwidth.
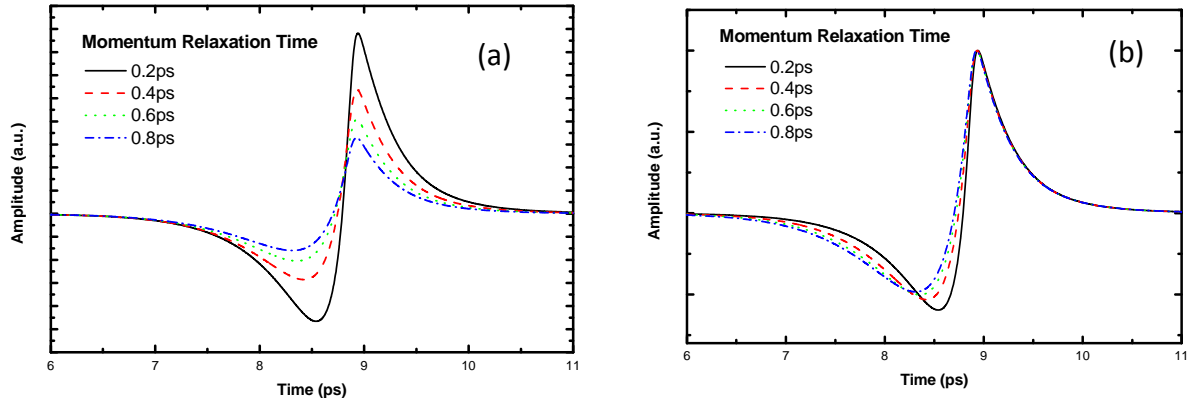
Figure 2-25 (a) Simulated THz fields sampling(without antenna response) with different materials at momentum relaxation time τ_s of 0.2ps, 0.4ps, 0.6ps, and 0.8ps, (b) normalize the peak amplitude of (a) to 1.
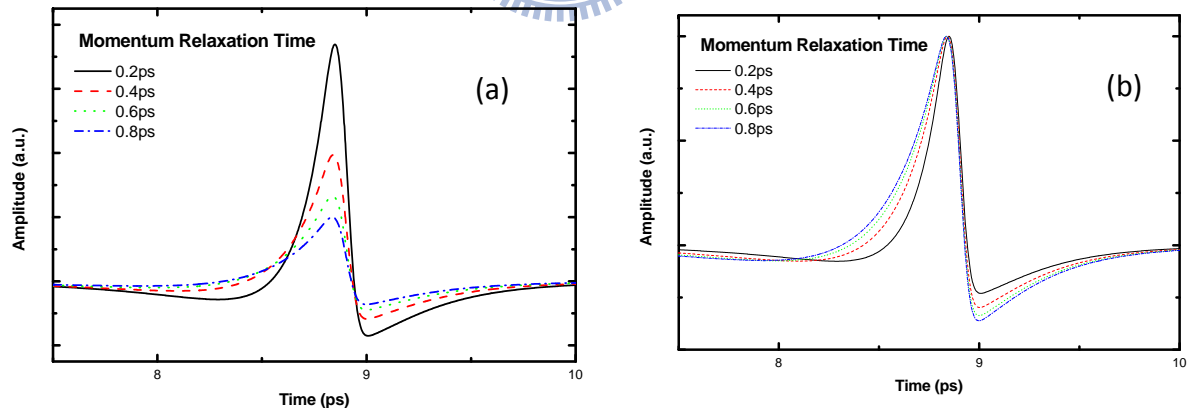
Figure 2-26 (a) Simulated THz fields sampling(with antenna response) with different materials at momentum relaxation time τ_s of 0.2ps, 0.4ps, 0.6ps, and 0.8ps, (b) normalize the peak amplitude of (a) to 1.

33

2.4 Conclusion

We concluded the role of carrier life time and momentum relaxation time in the generation and detection process in Table 2-2 and Table 2-3 respectively. From these tables, we can know how to choose suitable materials as THz emitter or detector for your applications. For example, if you only care about the power of your THz source, you can choose a material with slow carrier life time and slow momentum relaxation time as THz emitter, the other material with slow carrier life time and fast momentum relaxation time should be used as THz receiver.

THz emitter

		Emission Power	Emission Bandwidth
Carrier Life Time	Fast	Low	Broad
	Slow	High	Narrow
Momentum Relaxation Time	Fast	Low	Narrow
	Slow	High	Broader

Table 2-2 Comparison of carrier life time and momentum relaxation time in the generation process of THz field.

THz detector

		Receiving Power	Receiving Bandwidth
Carrier Life Time	Fast	Low	Broad
	Slow	High	Narrow
Momentum Relaxation Time	Fast	High	Broad
	Slow	Low	Narrow

Table 2-3 Comparison of carrier life time and momentum relaxation time in the detection process of THz field.

References

[1] M. Haner and W.S. Warren. "Generation of arbitrarily shaped picoseconds optical pulses using an integrated electro-optic waveguide modulator," Applied Optics, Vol. 26, pp. 3687-3694, Sep., 1987.

[2] J.P. Heritage, R.N. Thurston, W.J. Tomlinson, A.M. Weiner and R.H. Stolen, "Spectral windowing of frequency-modulated optical pulses in a grating compressor," Appl. Phys. Lett., Vol. 47, pp. 87-89, May, 1985.

[3] A.M. Weiner, D.E. Leaird, J.S. Patel, and J.R. Wullert, " Programmable femtosecond pulse shaping by use of a multielement liquid-crystal phase modulator," Opt. Lett., Vol. 15, pp. 326-328, Mar., 1990.

[4] M. A. Dugan, J. X. Tull, and W. S. Warren, "High-resolution acousto-optic shaping of unamplified and amplified femtosecond laser pulses," J. Opt. Soc. Am. B, Vol. 14, pp. 2348-2358, Sep., 1997.

[5] E. Zeek, K. Maginnis, S. Backus, U. Russek, M. Murnane, G. Mourou, H. Kapteyn, and G. Vdovin, "Pulse compression by use of deformable mirrors," Opt. Lett., Vol. 24, pp. 493-495, Apr., 1999.

[6] K Sala, G Kenney-Wallace, G Hall, "CW autocorrelation measurements of picosecond laser pulses," IEEE Journal of Quantum Electronics, Vol. 16, pp. 990-996, 1980.

[7] Rick Trebino, Kenneth W. DeLong, David N. Fittinghoff, John N. Sweetser, Marco A. Krumbügel, Bruce A. Richman, and Daniel J. Kane, "Measuring ultrashort laser pulses in the time-frequency domain using frequency-resolved optical gating," Rev. Sci. Instrum., Vo. 68, pp. 3277-3295, Sep., 1997.

[8] Y.L. Lin, C.K. Lee, and C.L. Pan, "An alternative approach to Frequency Resolved Optical Gating," PE-12, PSROC 2009.

[9] A. M. Weiner, "Femtosecond pulse shaping using spatial light modulators," Rev. Sci. Instrum., Vol. 71, pp. 1929-1960, May, 2000.

[10] A. Rundquist, A. Efimov, and D.H. Reitze, " Pulse shaping with the Gerchberg–Saxton algorithm," J. Opt. Soc. Am. B., Vol.19, pp. 2468-2478, Oct., 2002.

[11] D. Yelin, D. Meshulach, and Y. Silberberg, "Adaptive femtosecond pulse compression," Opt. Lett., Vol.22, pp.1793-1795, Dec., 1997.

[12] T. Baumert, T. Brixner, V. Seyfried, M. Strehle, G. Gerber, "Femtosecond pulse shaping by an evolutionary algorithm with feedback," Appl. Phys. B, Vol.65, pp. 779-782, Sep., 1997.

[13] M.C. Chen, J.Y. Huang, Q. Yang, C.L. Pan, and J.I. Chyi, "Freezing phase scheme for fast adaptive control and its application to characterization of femtosecond coherent optical pulses reflected from semiconductor saturable absorber mirrors," J. Opt. Soc. Am. B., Vo. 22, pp. 1134-1132, May, 2005.

[14] Z. Piao, M. Tani, and K. Sakai, "Carrier dynamics and terahertz radiation in photoconductive antennas," Jpn. J. Appl. Phys., Vol. 39, pp. 96-100, 2000.

[15] P. U. Jepsen, R.H. Jacobsen, and S.R. Keiding, "Generation and detection of terahertz pulses from bias semiconductor antennas," J. Opt. Soc. Am. B., Vol. 13, pp. 2424-2436, Nov., 1996.

[16] L. Duvillaret, F. Garet, J.F. Roux, and J.L. Coutaz, "Analytical modeling and optimization of terahertz time-domain spectroscopy experiments using photoswitches as antennas," IEEE J. STQE., Vol. 7, pp. 615-623, Jul./Aug., 2001.

[17] P.C. Upadhya, W.F. Andrew Burnett, J. Cunningham, A.G. Davies, E.H. Linfield, J. Lloyd-Hughes, E. Castro-Camus, M.B. Johnston, and H. Beere, "Excitation-density-dependent generation of broadband terahertz radiation in an asymmetrically excited photoconductive antenna," Opt. Lett., Vol. 32, pp. 2297-2299, Aug., 2007.

[18] G.C. Loata, "Investigation of low-temperature-grown GaAs photoconductive antennae

for continous-wave and pulsed terahertz generation," Ph.D. thesis, Goethe-University,

Frankfut am Main, 2007.

[19] J. C. Butcher, Numerical methods for ordinary differential equations, ISBN 0471967580

[20] Q. Wu and X.-C. Zhang, "Free-space electro-optic sampling of terahertz beams," App.

Phys. Lett., Vol. 67, pp. 3523-3525, Dec., 1995.

[21] S.G. Park and M.R. Melloch, "Analysis of terahertz waveforms measured by

photoconductive and electrooptic sampling," IEEE J. Quantum Electron., Vol. 35, pp. 810-819,

May, 1999.
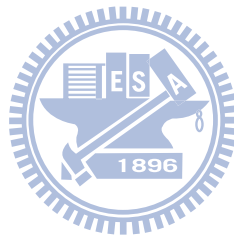
Chapter 3 Coherent Control of Terahertz Pulse Generation and Detection

In order to understand the role of chirp in the generation and detection processes of THz radiation, we utilize femtosecond pulse shaping technology in this study. This chapter can be divided into two parts : (1) coherent-control of pump pulse and probe pulse, (2) coherent control of both pump and probe pulse. The results are shown below.

3.1 Experiment Setup of Chirp-Controlled THz Time Domain System
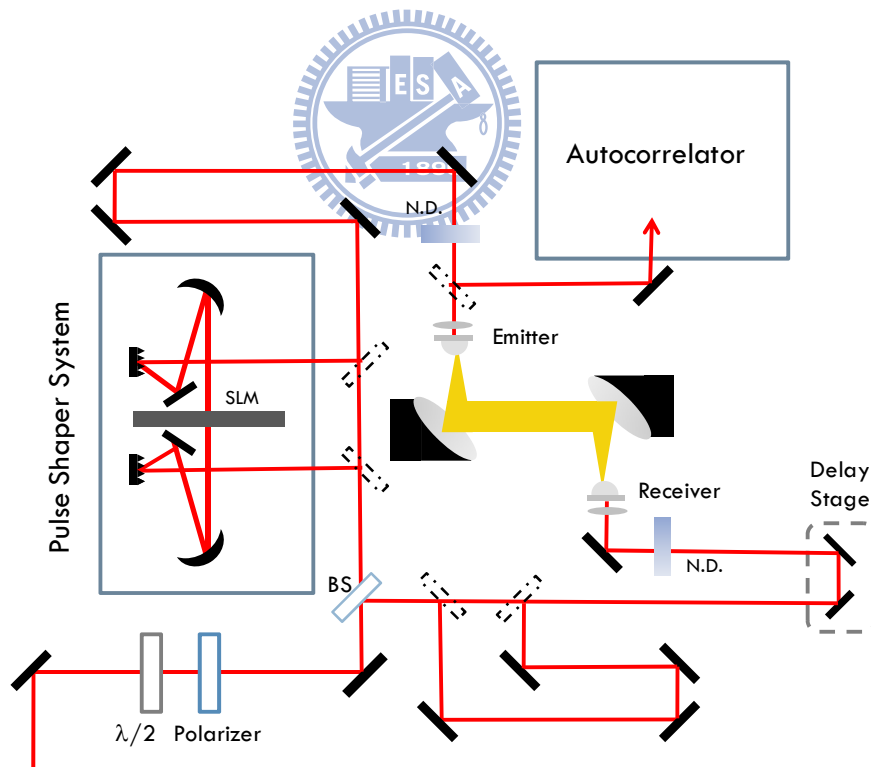
Figure 3-1 Experimental layout of chirp-controlled THz-Time Domain System (THz-TDS).

The experimental apparatus of the chirp-controlled THz Time Domain System is shown in Figure 3-1, the femtosecond laser pulse will pass through a half-wave plate and polarizer before entering the system, and it will be divided into two pulses by 50/50 beam splitter. One is pump pulse, and the other is probe pulse, the pump pulse will pass through a femtosecond laser pulse shaping system, which consists of a pair of gratings (600grooves/mm), two spherical reflectors with focal length 20cm, and a liquid crystal spatial light modulator with 128 pixels(SLM Cambridge Research and Instrumentation Inc. (CRI) Woburn, MA, SLM-128). We can provide different 2nd order spectra phase (chirp) to the pump pulse utilize this pulse shaping system.

The antenna we used in the experiment is low temperature grown GaAs (LT-GaAs) dipole antenna, which has fast carrier life time about 0.3ps, the time-domain signal of THz field is shown in Figure 3-2, the FWHM of the THz pulse is about 1.06ps, and the efficient bandwidth is about 2.5THz. From Figure 3-2 (b), we can find out there are several absorption dips in the power spectrum, as 0.567THz, 1.103THz, 1.406THz, and 1.69THz, which is due to the absorption of water vapor[2-3].

(a)

(b)
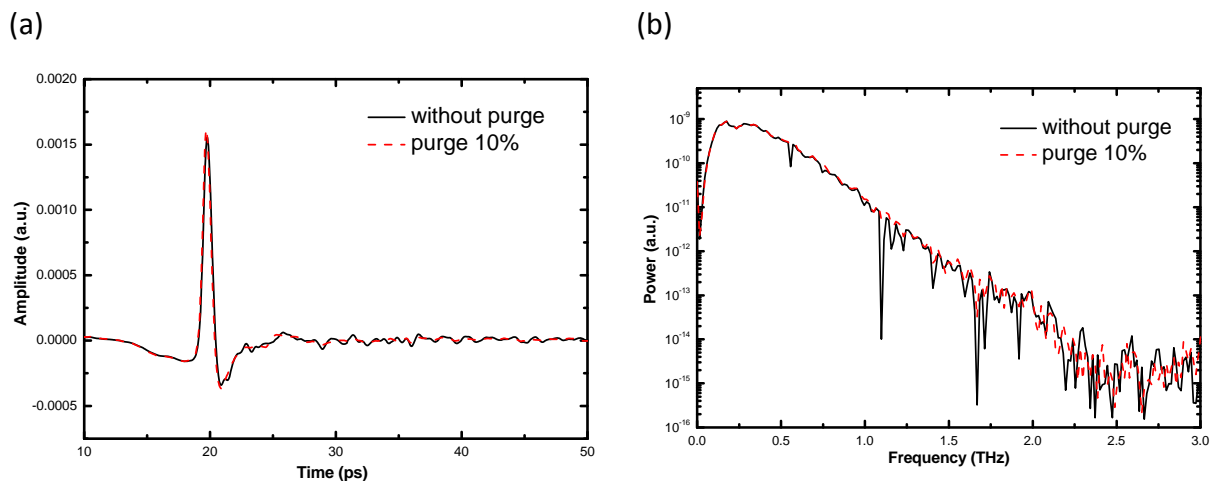
Figure 3-2 (a) Time domain THz field without purge, and purged with 10% nitrogen, (b) power spectrum.

3.2 THz Generation under Different Chirp Pulses

First, we study the generation mechanism of THz field under different chirped pulses. The pump power and probe power of the laser are 30mW and 20mW respectively. The pump pulse is controlled by the pulse shaping system, while the probe pulse is without control, the experiment results are shown below.

3.2.1 Experiment Results

Pumping with Positively Chirped Pulses
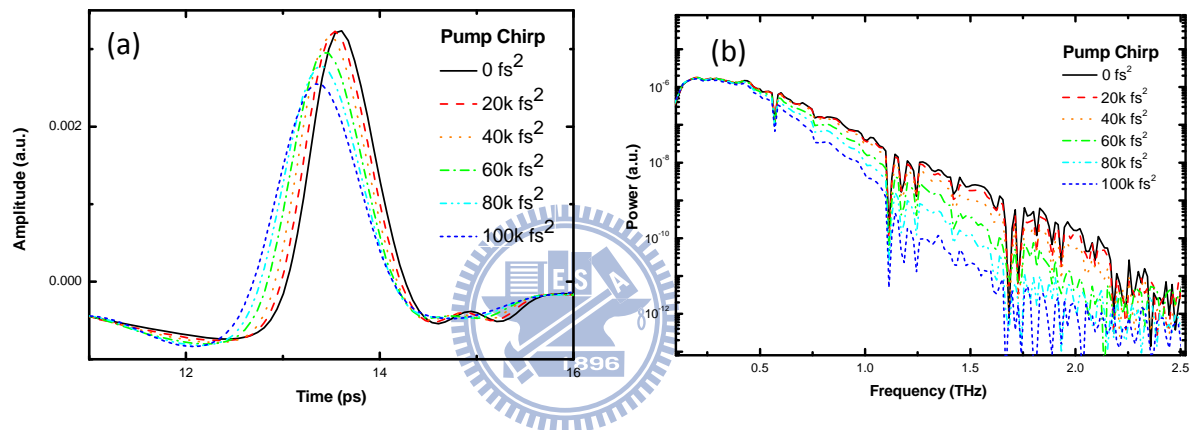
Figure 3-3 (a) Time domain profile of the THz field generated with different positively chirped pulses, and (b) the power spectrum.

Pumping with Negatively Chirped Pulses
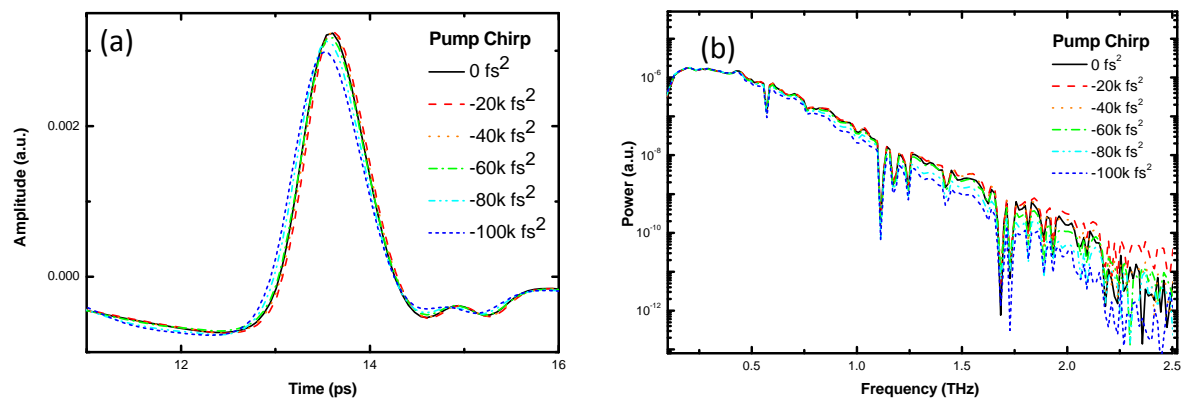
Figure 3-4 (a) Time domain profile of the THz field generated with different negatively chirped pulses, and (b) the power spectrum.
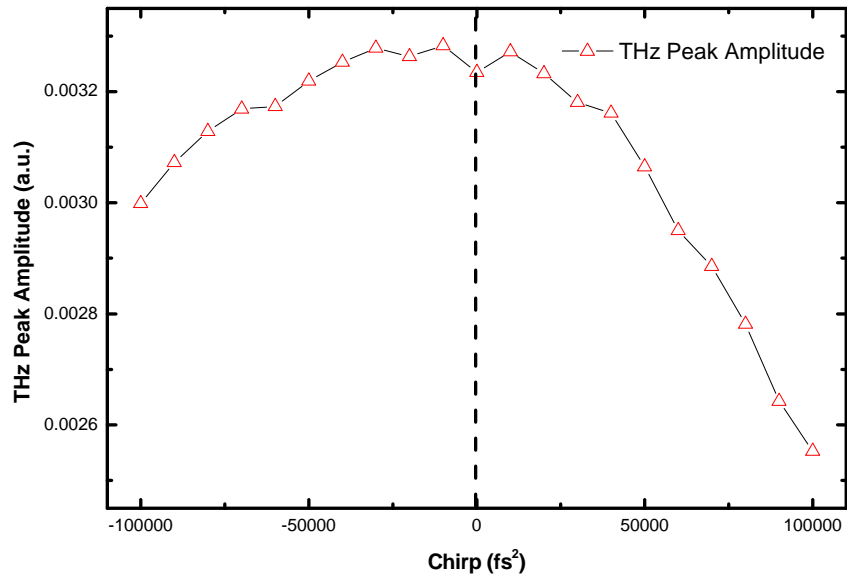
Figure 3-5 THz Peak Amplitude v.s. chirp of the pump pulses.

From the experiment results above, we can find out the extreme different behaviors between positive chirp excitation and negative chirp excitation. The maximum peak amplitude of THz pulse is not located at zero chirp, and the THz peak amplitude is very sensitive to the positive chirp, when we increase the quantities of the chirp, the positive chirped pulse will have lower THz peak amplitude than the negative chirped pulse.

3.2.2 Discussion

The experiment results show that the slightly positive chirped pulse will have maximum THz peak amplitude, it may due to the relationship between carrier life time and laser chirp. From Figure 1-2, we can know that the positive chirped pulse excitation will have longer carrier life time than the negatively chirped pulse, and from the simulation results in Figure 2-15, we can know that the material with longer carrier life time will have maximum THz peak amplitude. The other possible influence may contribute to the

41

Intra pulse Pump Down Process (**IPDP**) [4-5], as shown in Figure 3-6.
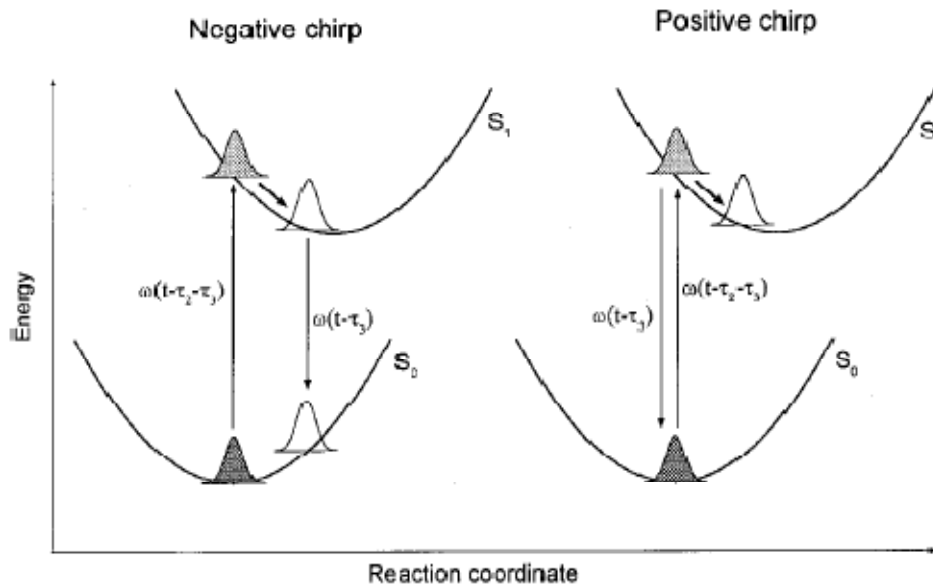
Figure 3-6 Diagrams of the pump-dump process for negatively chirped (NC) pulse and

positively chirped (PC) pulse excitation [4].

The interaction of an optical pulse with such a system can be thought of in terms of sequential interactions with the field. A negatively chirped pulse can be represents as a sequence of frequency components from high to low, when the first photon excite the carriers from valance band (VB) to the conduction band (CB), the carriers will move from higher to lower energy along the CB, when the second photon with lower energy entering the system, it may induce stimulated emission, and the carriers in the CB will be reduced, it is called "pump-dump" process. A positively chirped pulse cannot enhance the stimulated emission process, so the positively chirped pulse will generate more carriers than the NC pulses.

3.3 THz Detection under Different Chirped Pulses

The role of chirp in the detection processes of THz field is discussed in this section. We study the detection mechanism of THz field under different chirped pulses. The pump power and probe power of the laser are 30mW and 20mW respectively. The probe pulse is controlled by the pulse shaping system, while the pump pulse is without control, the experiment results are shown below.

3.3.1 Experiment Results

Sampling with Positively Chirped Pulses
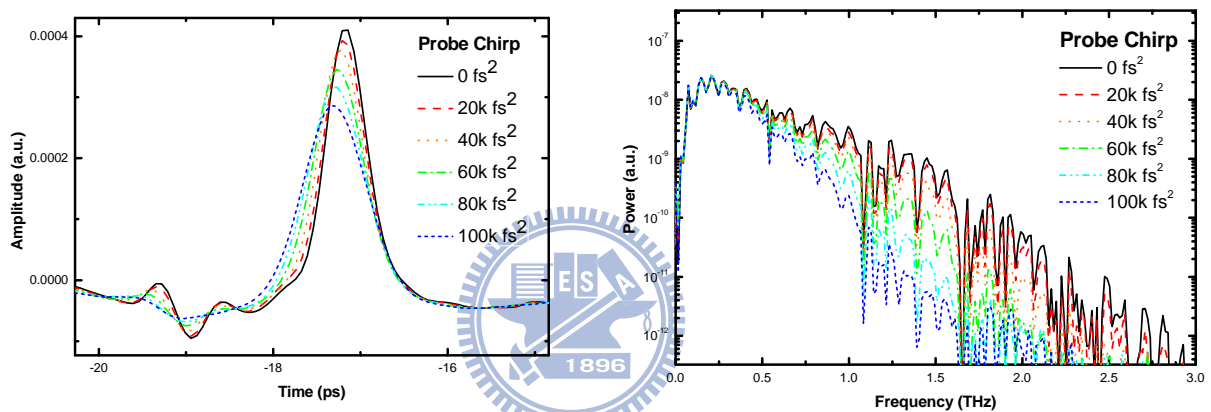
Figure 3-7 (a) Time domain profile of the THz field sampling with different positively chirped pulses, and (b) the power spectrum.

Sampling with Negatively Chirped Pulses
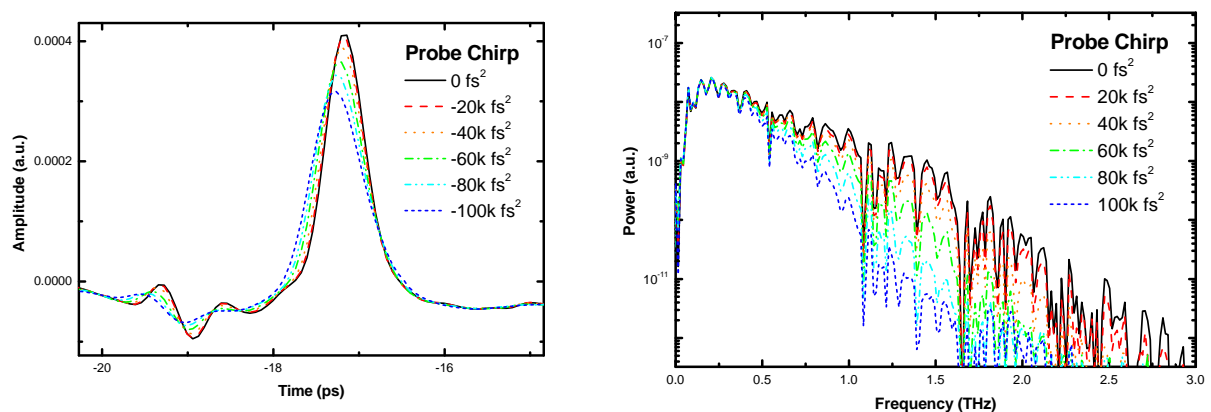
Figure 3-8 (a) Time domain profile of the THz field sampling with different negatively chirped pulses, and (b) the power spectrum.
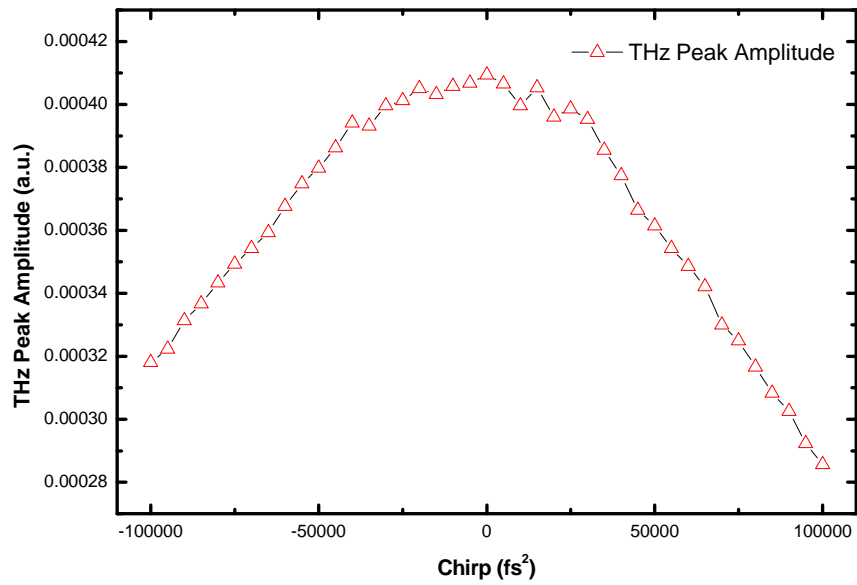
Figure 3-9 THz Peak Amplitude v.s. chirp of the pump pulses.

In the detection process, we can also find out the asymmetry behaviors between positively chirped pulses and negatively chirped pulses. However, unlike the generation process, the detected THz field will have maximum peak amplitude value in zero chirped case.

3.3.2 Simulation Results and Discussion

The asymmetry behaviors in the detection process may due to the relationship between the laser chirp and carrier life time and momentum relaxation time. If the carrier life time and momentum relaxation time is independent of chirp, the only problem we must consider is the gating pulse width. Figure 3-10 shows the simulation results of the relationship between THz peak amplitude and laser chirp, the carrier life time and momentum relaxation is independent of chirp in this simulation.
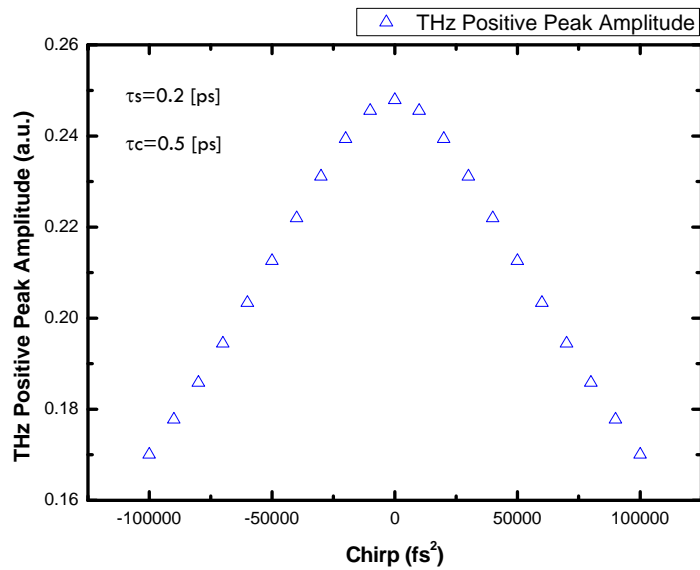
Figure 3-10 Simulation results of THz peak amplitude v.s. the chirp of the gating pulses, carrier life and momentum relaxation time is independent of chirp in this case.
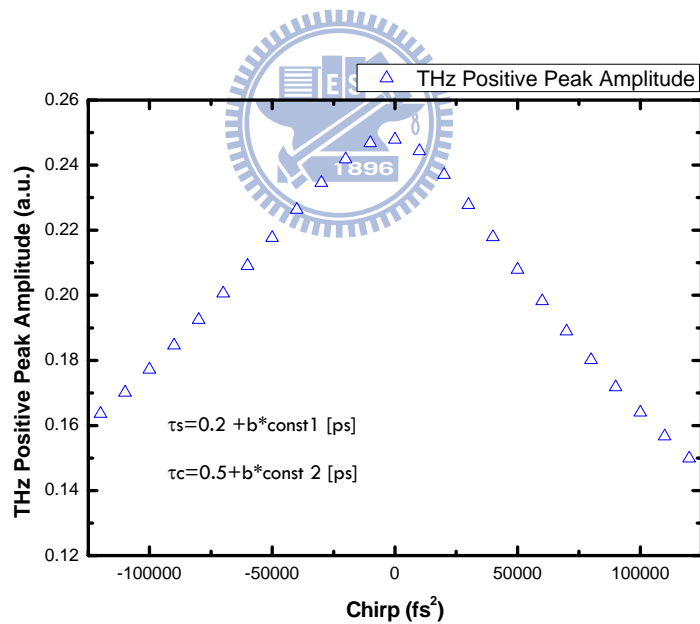
Figure 3-11 Simulation results of THz peak amplitude v.s. the chirp of the gating pulses, carrier life and momentum relaxation time is linear dependent of chirp in this case.

Figure 3-11 shows the results simulation results considering the relationship between chirp and carrier life time and momentum relaxation time, the simulation results show the asymmetry behaviors, which is same as our experimental results.

3.4 Simultaneous Chirp Control of Both Pump Pulse and Probe Pulse

From the previous discuss, we can found that the asymmetry behavior of chirp dependence in the generation and detection process, while the experiment above only control only pump pulses or probe pulses respectively, how about control the pump and probe pulse simultaneously ? In this section, we will show the experiment results of simultaneous chirp control of both pump pulse and probe pulse.

3.4.1 Experiment Setup
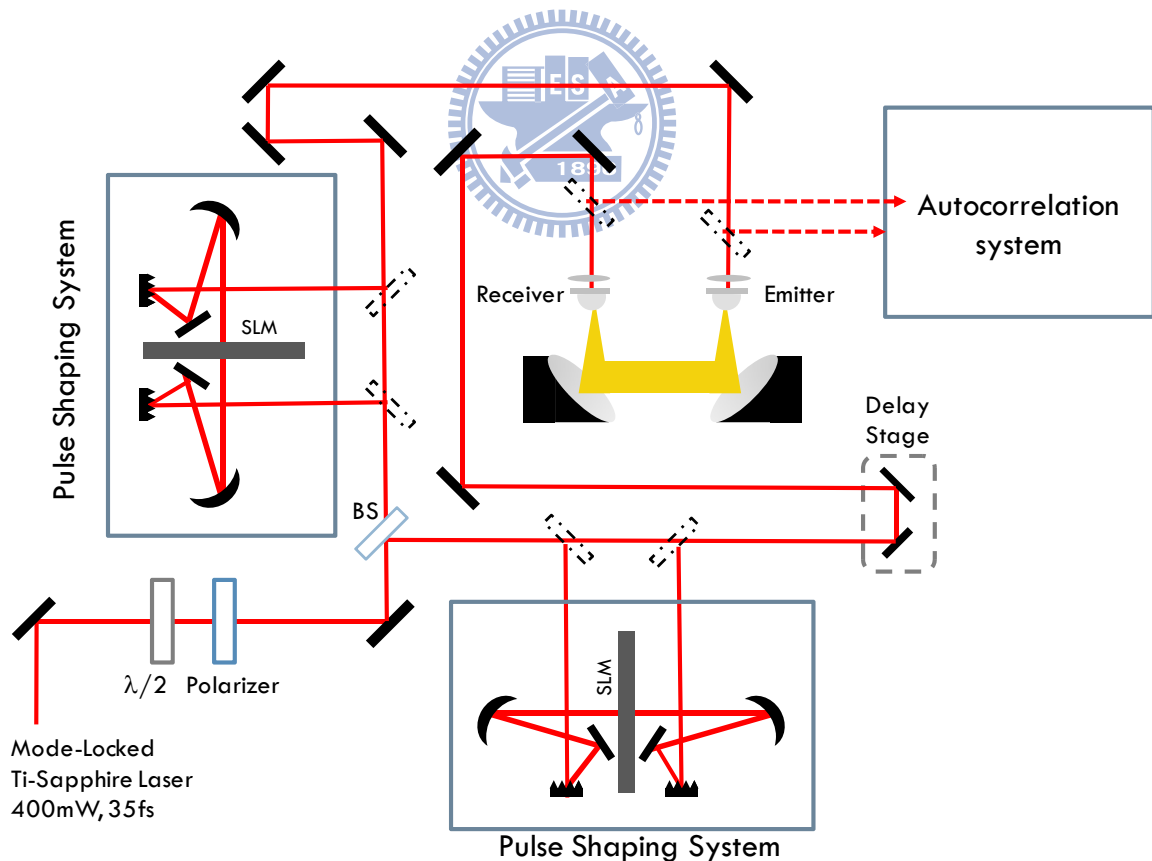
Figure 3-12 Experimental setup of coherent-controlled THz –time domain system.

Figure 3-12 shows the experiment setup of the coherent-controlled THz-TDS, both pump pulse and probe pulse are coherent-controlled by pulse shaping system, the pulse shaping system was tested with the autocorrelation measurement system before experiment.

3.4.2 Results and Discussion

Figure 3-13 shows a traditional THz waveform generated from LT-GaAs dipole antenna, which has three significant features : (a) Positive peak amplitude (b) 1st negative peak amplitude and (c) 2nd negative peak amplitude, which has different physical meanings.
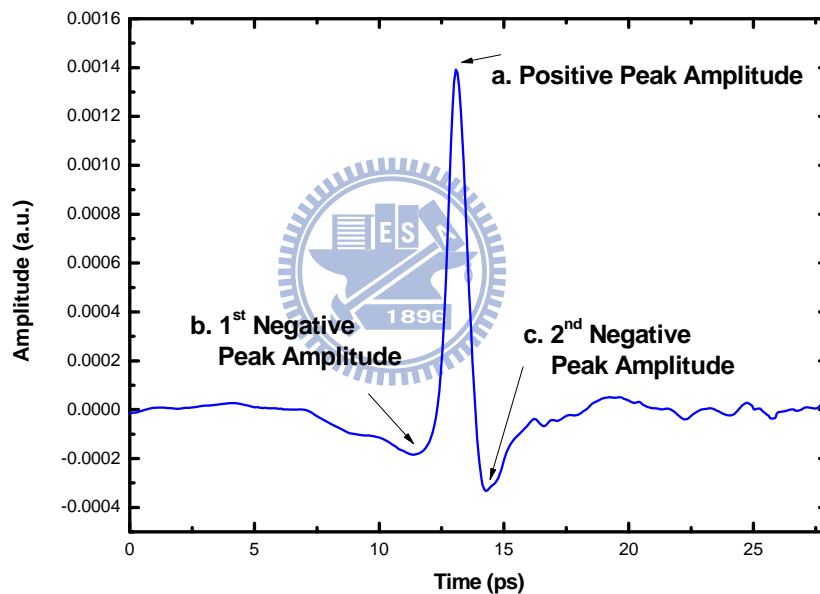
Figure 3-13 THz waveform.

In this experiment, we change the chirp of the pump pulse and probe pulse from -400k fs^2 to +400k fs^2, the chirp spacing in the experiment is 20k fs^2, which measured 41×41 THz waveforms in the experiment, we made different control plots to discuss the experiment results below.

A. Positive Peak Amplitude of THz pulse
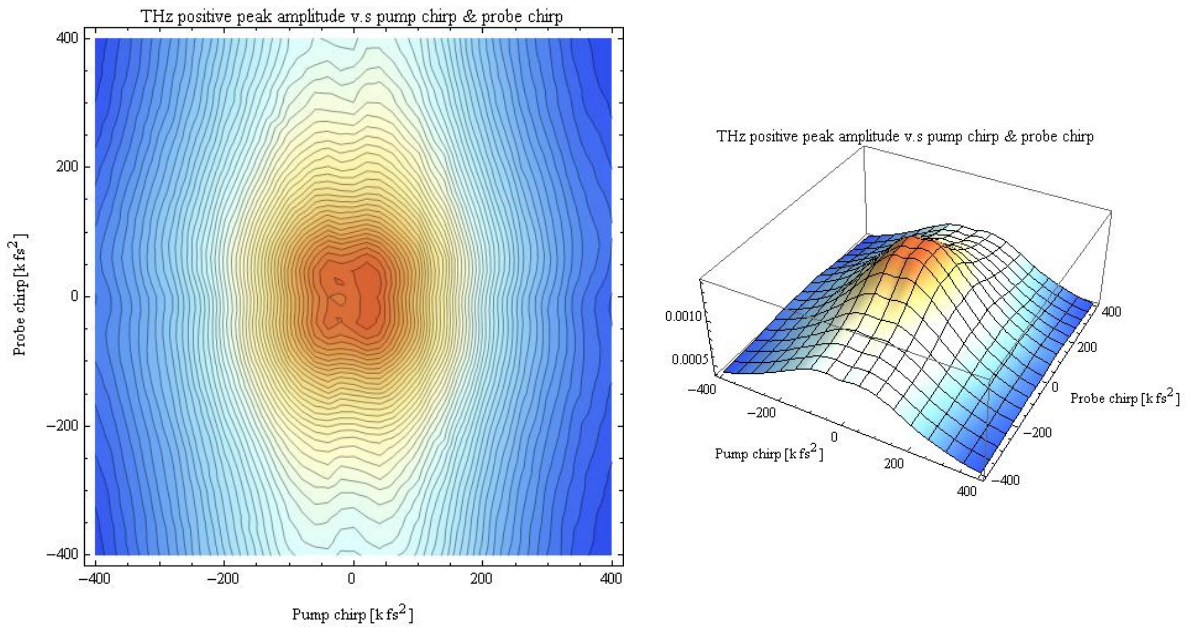
Figure 3-14 THz positive peak amplitude v.s. pump chirp & probe chirp.

The positive peak amplitude is associated with the total power of the THz field, from the experiment results, we can found out the asymmetry behaviors between positively chirped and negatively chirped pulses. The pump pulse with positively chirp will have maximum THz peak amplitude, Figure 3-15 shows the results of the THz peak amplitude v.s. pump chirp at different probe chirps. The dip located in the zero chirp is due to the two photon absorption effect, which will reduce the emission power of the THz wave.
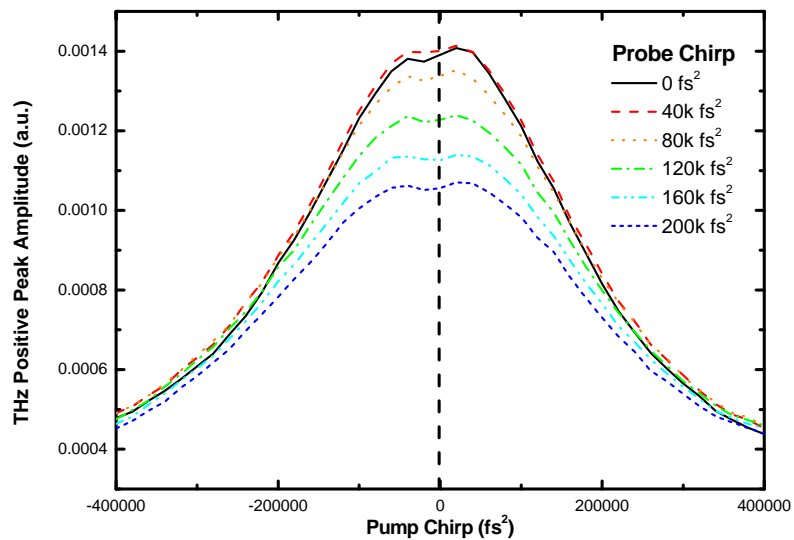
Figure 3-15 THz Peak Amplitude v.s. pump chirp at different probe chirps.

B. 1st Negative Peak Amplitude of THz pulse
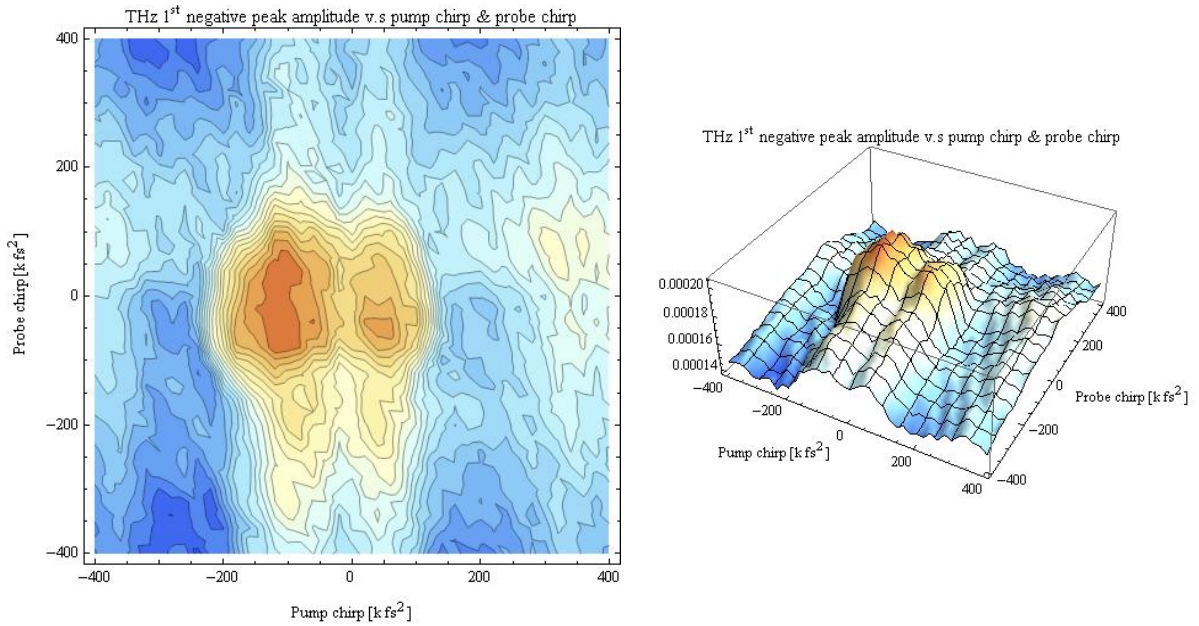
Figure 3-16 THz 1st negative peak amplitude v.s. pump chirp & probe chirp.

The origin of the 1st negative peak is due to the sampling effect and antenna response [6], the dependence of probe chirp is nearly symmetry, from Figure 3-16, we can find out the interesting behavior that pump with negatively chirped pulse will generate maximum value of 1st negative peak. It's consistent with the chirp dependence of positive peak amplitude and the conservation of energy, where the maximum positive peak amplitude occurs at positively chirp pulse.

C. 2nd Negative Peak Amplitude of THz pulse

The 2nd negative peak is corresponding to the carrier relaxation process [7], we can find out the pump chirp dependence of the 2nd negative peak is nearly symmetry from Figure 3-17, however, it's very sensitive to the probe chirp, the dependence of the probe pulse shows a valley like shape and have a dip in the zero chirp region, this behavior is similar to the chirp dependence of the THz positive peak amplitude. The origin of this dip is not two photon absorption effect, it's due to the sampling effects : (1) From the discussions & simulations in Chapter 2.3, we can know that the longer the carrier relaxation time, the higher the THz

49

positive peak amplitude and 2nd negative peak amplitude, and with the same quantity of chirp, positive chirp pulse will have longer carrier life time than the negative one. (2) The higher the laser chirp, the longer the pulse width, and the long pulse width will reduce the measured THz values. According to (1) and (2) , we can got the experiment results below.
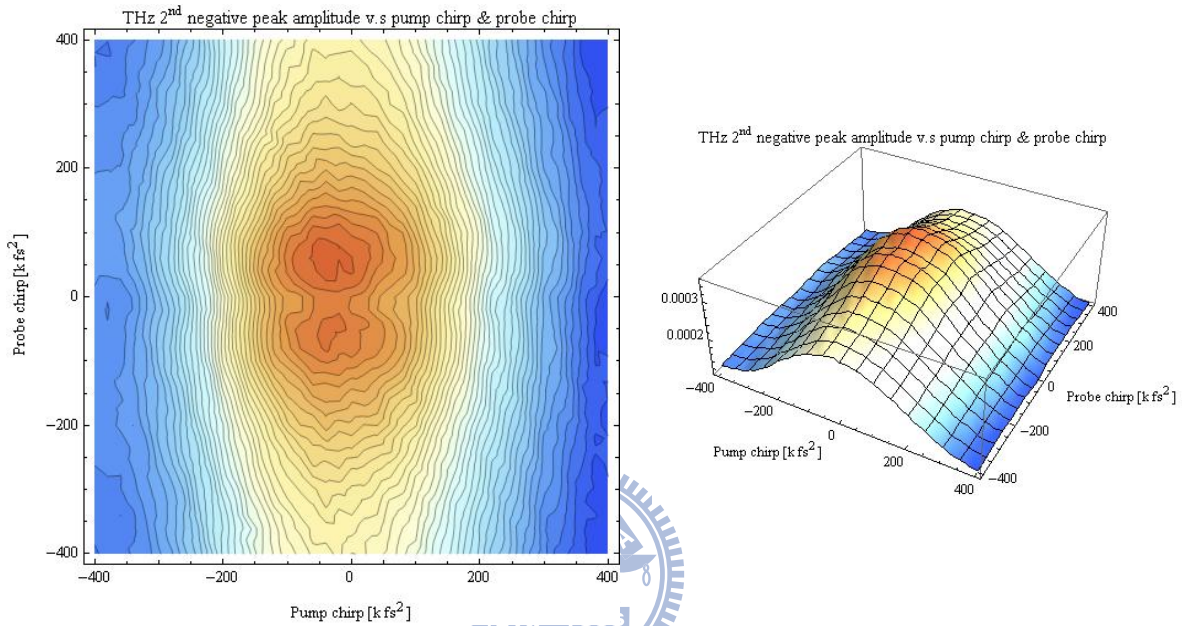
Figure 3-17 THz 2nd negative peak amplitude v.s. pump chirp & probe chirp.

D. Total Power of THz pulse
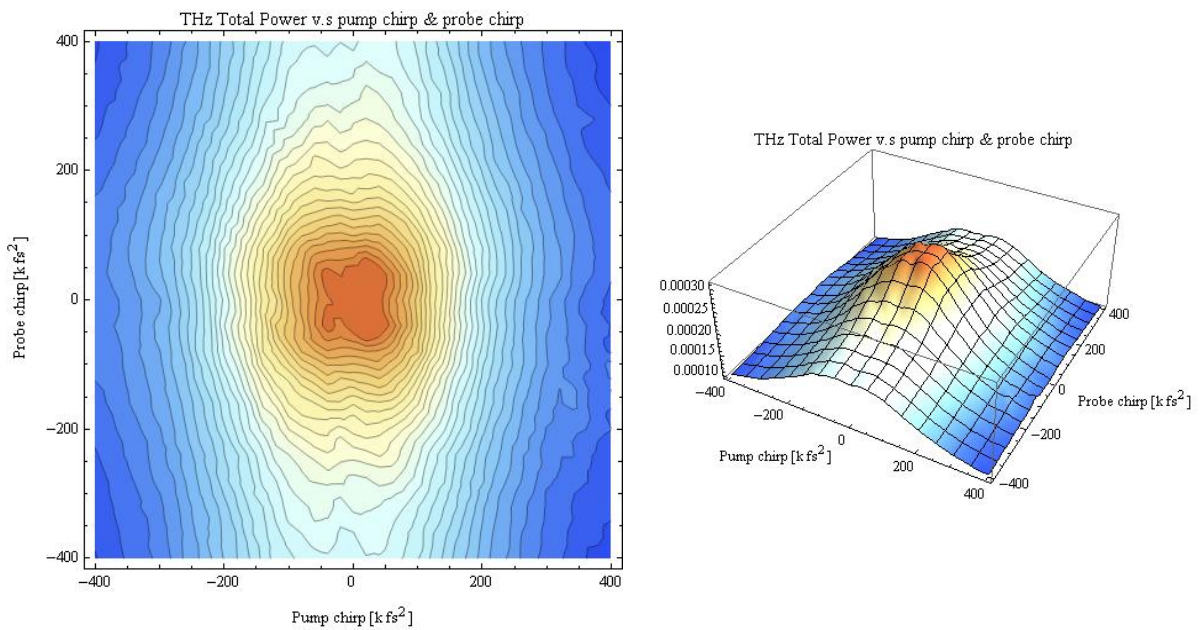
Figure 3-18 THz total power v.s. pump chirp & probe chirp.

Power Dependence
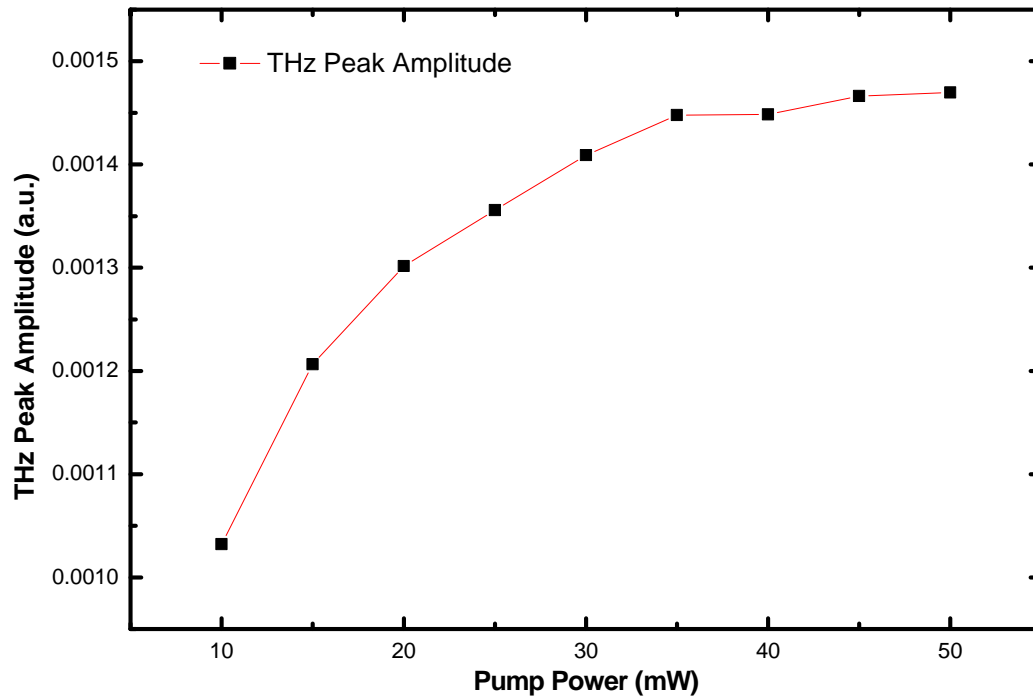
Figure 3-19 THz Peak amplitude v.s. pump power.

The chirp dependence of the total power of THz radiation is shown in Figure 3-18, it shows

the tendency that if we pump and probe with slightly positively chirped pulse, we will get

maximum THz total power, it's consistent with our previously works, and the power

dependence of the THz peak amplitude is shown in Figure 3-19, the THz peak amplitude will

saturated when the pump power greater than 35mW, this experiment is done without chirp

control.

3.5 Conclusion

From the experiments above, we can find out the asymmetry behaviors between positively chirped pulse and negatively chirped pulses in the excitation and detection process of THz radiation. There were a dip in the zero chirp both in the pump chirp case and probe chirp case. It may due to the two photon absorption effect, the zero chirped pulse will have maximum excitation power than the chirped pulses, and this two photon absorption effect will reduce the effective carriers both in the excitation or detection process, so the peak amplitude of the THz radiation will reduced when we excited or gating with zero chirped pulses.

In this chapter, we utilize the pulse shaping system to discuss the role of chirp in the excitation and detection process of THz radiation, the experimental results is consistent with the theoretical simulation, and the two-photon absorption effect is also observed.

References

[1] S.H. Lin, "The Study of Terahertz Radiation Mechanism from Photoconductive Antenna by Femtosecond Pulse Shaping Technology," Master Thesis, NCTU.

[2] M Exter, C Fattinger, D Grischkowsky, "Terahertz time-domain spectroscopy of water vapor," Opt. Lett., Vol. 14, pp. 1128-1130, Oct., 1989.

[3] L. Thrane, R.H. Jacobsen, P. Uhd Jepsen and S.R. Keiding, "THz reflection spectroscopy of liquid water," Chem. Phys. Lett., Vol. 240, pp. 330-333, Jun., 1995.

[4] B.D. Fainberg, and V.A. Gorbunov, "Coherent population transfer in molecules coupled with a dissipative environment by an intense ultrashort chirped pulse," J. Chem. Phys., Vol. 117, pp. 7222-7232, Oct., 2002.

[5] B.D. Fainberg, B. Levinsky, and V.A. Gorbunov, "Chirped-pulse control of carriers in semiconductors : the role of many-body effect," J. Opt. Soc. Am. B, Vol.22, pp. 2715-2727, Dec., 2005.

[6] P. U. Jepsen, R.H. Jacobsen, S.R. Keiding, "Generation and detection of terahertz pulses from biased semiconductor antennas," J. Opt. Soc. Am. B, Vol.13, pp. 2424-2436, Nov., 1996.

[7] M. Tani, S. Matsurra, K. Sakai, S.I. Nakashima, "Emission characteristics of photoconductive antennas based on low-temperature-grown GaAs and semi-insulating GaAs," Appl. Opt., Vol. 36, pp. 7853-7859, Oct., 1997.

Chapter 4. A Chirp-controlled THz Time Domain Spectrometer

From the previous study, we can know that the laser chirp influence on THz generation and detection process, in this chapter, we will focus the influence of chirp on THz time domain spectrometer in this chapter.

4.1 Material Optical Constants Extraction from Terahertz Time Domain Spectroscopy

The method to extract material optical constants from THz-TDS is based on measuring the effects on the electric field of a THz wave pass through investigated material. The temporal profile of the THz pulse which pass through the material is measured as $E_{sig}(t)$, and the other THz pulse without pass through the material is measured as $E_{ref}(t)$. This two signals will be transfer to frequency domain by Fourier transform, and the transfer function is determined by their quotient :

$$\widetilde{H}_{\exp}(\omega) = \frac{\widetilde{E}_{sig}(\omega)}{\widetilde{E}_{ref}(\omega)} \tag{4.1}$$

Since the material constants cannot direct compute from the complex transfer function directly, this is called an inverse problem, some algorithms [1-3] will be used to make the theoretically derived transfer function $\widetilde{H}_{theory}(\omega)$ equal to the experimental transfer function $\widetilde{H}_{\exp}(\omega)$, we will introduce the method we used in the following section.

4.1.1 Method of Extraction Optical Constants from Thick Samples
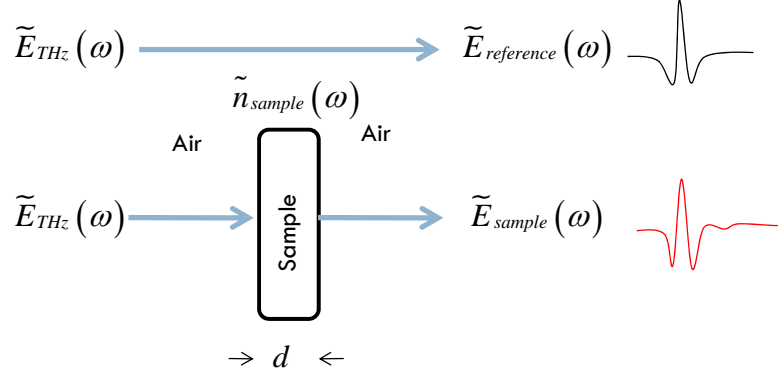
Figure 4-1 Schematic of electromagnetic model for thick sample.

If the sample which we want to measure is thick enough (typically >100 m), the reflection signal is clearly separated in time-domain, and the Fabry-Perot effect could be ignore, it could simply the material constants retrieval process. The reference field can be express by

$$\widetilde{E}_{reference}(\omega) = \widetilde{E}_{THz}(\omega)\exp\left[-j\frac{\omega\widetilde{n}_{air}(\omega)d}{c_0}\right] \tag{4.2}$$

Where $\widetilde{n}_{air} = 1.00027 - j0$ is the refractive index of air, d is the thickness of sample, $c_0 = 299792458$ [m/s] is the speed of light in vacuum. The signal field which passed through the sample we want to measure can be expressed by

$$\widetilde{E}_{sample}(\omega) = \widetilde{E}_{THz}(\omega)\widetilde{t}_{12}(\omega)\exp\left[-j\frac{\omega\widetilde{n}_{sample}(\omega)d}{c_0}\right]\widetilde{t}_{21}(\omega) \tag{4.3}$$

Where $\widetilde{t}_{12}(\omega)$ and $\widetilde{t}_{21}(\omega)$ are the Fresnel transmission coefficient, it can be expressed by

$$\widetilde{t}_{12}(\omega) = \frac{2\widetilde{n}_{air}(\omega)}{\widetilde{n}_{air}(\omega) + \widetilde{n}_{sample}(\omega)} \tag{4.4}$$

$$\widetilde{t}_{21}(\omega) = \frac{2\widetilde{n}_{sample}(\omega)}{\widetilde{n}_{air}(\omega) + \widetilde{n}_{sample}(\omega)} \tag{4.5}$$

The complex refractive index of the sample can be written as

$$\tilde{n}_{sample}(\omega) = n_s(\omega) - j\kappa_s(\omega) \tag{4.6}$$

Where $n_s(\omega)$ is the real refractive index and $\kappa_s(\omega)$ is the extinction coefficient indicating the absorption, the relationship between absorption coefficient $\alpha_s(\omega)$ and extinction coefficient $\kappa_s(\omega)$ is :

$$\kappa_s(\omega) = \frac{\alpha_s(\omega)c_0}{2\omega} \tag{4.7}$$

From equation (4.1) to equation (4.5), we can get the theoretical transfer function :

$$\tilde{T}(\omega) = \frac{\tilde{E}_{sample}(\omega)}{\tilde{E}_{reference}(\omega)} = \tilde{t}_{12}(\omega)\tilde{t}_{21}(\omega)\exp\left[-j\frac{\omega d}{c_0}\left(\tilde{n}_{sample}(\omega) - \tilde{n}_{air}(\omega)\right)\right]$$

$$= \frac{4\tilde{n}_{air}(\omega)\tilde{n}_{sample}(\omega)}{\left[\tilde{n}_{air}(\omega) + \tilde{n}_{sample}(\omega)\right]^2}\exp\left[-j\frac{\omega d}{c_0}\left(\tilde{n}_{sample}(\omega) - \tilde{n}_{air}(\omega)\right)\right] \tag{4.8}$$

Assume the absorption of the material is less than the real part of the refractive index ($\kappa_s \ll n_s$), we could simplify the transfer function to

$$\tilde{T}(\omega) = \frac{4n_{air}n_s(\omega)}{\left[n_{air} + n_s(\omega)\right]^2}\exp\left[-j\frac{\omega d}{c_0}\left(n_s(\omega) - j\kappa_s(\omega) - n_s(\omega)\right)\right]$$

$$= \frac{4n_{air}n_s(\omega)}{\left[n_{air} + n_s(\omega)\right]^2}\exp\left[-\frac{\omega d}{c_0}\kappa_s(\omega)\right]\exp\left[-j\frac{\omega d}{c_0}\left(n_s(\omega) - n_{air}\right)\right] \tag{4.9}$$

$$= \rho(\omega)\exp\left[j\Delta\phi(\omega)\right]$$

The real part of the refractive index could be calculated by the phase difference $\Delta\phi(\omega)$:

$$n_s(\omega) = n_{air} - \frac{c_0\Delta\phi(\omega)}{\omega d} \tag{4.10}$$

After get the real part of refractive index from equation (4.10), the extinction coefficient $\kappa_s(\omega)$ also can be obtained from equation (4.9) :

$$\kappa_s(\omega) = -\frac{c_0}{\omega d} \ln\left[\frac{\rho(\omega)\left(n_{air} + n_s(\omega)\right)^2}{4 n_{air} n_s(\omega)}\right] \tag{4.11}$$

From the calculation above, we could extract frequency dependent complex refractive index from the experiment.

4.1.2 Problems of Photoconductive Antenna Sampling Effect

In the experiment, the most popular THz-TDS is based on photoconductive antenna pair system, which is easy to buildup than EO sampling system. Unlike the traditional spectrometer, which measures the frequency spectrum by means of expand the frequency spectrum into spatially separated components by diffraction grating and recorded it by a CCD camera, THz Time Domain Spectroscopy is based on Fourier transform spectroscopy, which doesn't measure the frequency response directly, the spectrum is calculated from the Fourier transform of the time-domain profile measured in the experiment.

For the applications of spectroscopy, we must take care of what we really measure in the experiment, otherwise we will get wrong information during the Fourier transform process, from the discussion above, the material constant retrieval is based on transfer function of sample signal and reference signal in the frequency domain :

$$\widetilde{M}(\omega) = \frac{\widetilde{E}_{sample}(\omega)}{\widetilde{E}_{reference}(\omega)} = \frac{F\{\widetilde{E}_{sample}(t)\}}{F\{\widetilde{E}_{reference}(t)\}} = \frac{\int_{-\infty}^{\infty} \widetilde{E}_{sample}(t)\exp[-j\omega t]dt}{\int_{-\infty}^{\infty} \widetilde{E}_{reference}(t)\exp[-j\omega t]dt} \tag{4.11}$$

The signal we measured by PC antenna $\widetilde{E}^M(\tau)$ which is the correlation of time-dependent conductance $g(t)$ and the time-domain electric field on the detection antenna :

$$\widetilde{E}_{sample}^M(\tau) = \int_{-\infty}^{\infty} \widetilde{E}_{sample}(t)\,g(t-\tau)dt \tag{4.12}$$

$$\widetilde{E}_{reference}^M(\tau) = \int_{-\infty}^{\infty} \widetilde{E}_{reference}(t)\,g(t-\tau)dt \tag{4.13}$$

Where $\widetilde{E}_{sample}(t)$ is the time domain electric field with material response on the detector

antenna, and $\widetilde{E}_{reference}(t)$ is the reference electric field on the antenna. The electric field with

sample response can be represented by

$$\widetilde{E}_{sample}(t) = F^{-1}\left\{\widetilde{E}_{THz}(\omega)H_a(\omega)H_m(\omega)\right\}$$ (4.14)

Where $\widetilde{E}_{THz}(\omega)$ is the THz field generated from the PC antenna, $H_a(\omega)$ is the antenna

response, and $H_m(\omega)$ is the material response, the reference signal also carries the antenna

response :

$$\widetilde{E}_{reference}(t) = F^{-1}\left\{\widetilde{E}_{THz}(\omega)H_a(\omega)\right\}$$ (4.15)

Combine equation (4.11) to equation (4.15), we will get :

$$\widetilde{M}(\omega) = \frac{F\left\{\widetilde{E}_{sample}^{M}(t)\right\}}{F\left\{\widetilde{E}_{reference}^{M}(t)\right\}} = \frac{F\left\{\int_{-\infty}^{\infty}\widetilde{E}_{sample}(t)g(t-\tau)dt\right\}}{F\left\{\int_{-\infty}^{\infty}\widetilde{E}_{reference}(t)g(t-\tau)dt\right\}}$$

$$= \frac{\int_{-\infty}^{\infty}\left\{\int_{-\infty}^{\infty}\widetilde{E}_{sample}(t)g(t-\tau)dt\right\}e^{-j\omega\tau}d\tau}{\int_{-\infty}^{\infty}\left\{\int_{-\infty}^{\infty}\widetilde{E}_{reference}(t)g(t-\tau)dt\right\}e^{-j\omega\tau}d\tau}$$ (4.16)

The correlation process of the conductance and THz field will prohibit us retrieval the actual

material properties. There are two cases that we can reduce the correlation effect :

(1) If the time-dependence conductance is a delta-function, $g(t) = \delta(t)$, equation (4.16) can

   be reduce to

$$\widetilde{M}(\omega) = \frac{\int_{-\infty}^{\infty}\left\{\int_{-\infty}^{\infty}\widetilde{E}_{sample}(t)\delta(t-\tau)dt\right\}e^{-j\omega\tau}d\tau}{\int_{-\infty}^{\infty}\left\{\int_{-\infty}^{\infty}\widetilde{E}_{reference}(t)\delta(t-\tau)dt\right\}e^{-j\omega\tau}d\tau} = \frac{\int_{-\infty}^{\infty}\widetilde{E}_{sample}(\tau)e^{-j\omega\tau}d\tau}{\int_{-\infty}^{\infty}\widetilde{E}_{reference}(\tau)e^{-j\omega\tau}d\tau}$$ (4.17)

$$= \frac{\widetilde{E}_{THz}(\omega)H_a(\omega)H_m(\omega)}{\widetilde{E}_{THz}(\omega)H_a(\omega)} = H_m(\omega)$$

(2) If the temporal profile of the conductance is symmetry : $g(t) = g(-t)$, the correlation process is equal to convolution process

$$\int_{-\infty}^{\infty} \widetilde{E}(t) g(t-\tau) dt = \int_{-\infty}^{\infty} \widetilde{E}(t) g(\tau-t) dt = \widetilde{E}(t) \otimes g(t) \tag{4.18}$$

The convolution of THz field and conductance can be eliminated during the Fourier Transform process :

$$\widetilde{M}(\omega) = \frac{F\left\{\widetilde{E}_{sample}^{M}(t)\right\}}{F\left\{\widetilde{E}_{reference}^{M}(t)\right\}} = \frac{F\left\{\widetilde{E}_{sample}(t) \otimes g(t)\right\}}{F\left\{\widetilde{E}_{reference}(t) \otimes g(t)\right\}}$$

$$= \frac{F\left\{\widetilde{E}_{sample}(t)\right\} F\left\{g(t)\right\}}{F\left\{\widetilde{E}_{reference}(t)\right\} F\left\{g(t)\right\}} = \frac{\widetilde{E}_{THz}(\omega) H_a(\omega) H_m(\omega) F\left\{g(t)\right\}}{\widetilde{E}_{THz}(\omega) H_a(\omega) F\left\{g(t)\right\}} \tag{4.19}$$

$$= H_m(\omega)$$

Recall the time-dependence conductance introduced in chapter 2 :

$$g(t) = \int^{t} dt' I_g(t') \left(1 - e^{-\frac{(t-t')}{\tau_S}} \right) e^{-\frac{(t-t')}{\tau_C}} \tag{2.24}$$

The temporal profile of the conductance is asymmetric in nature, due to the fast photocurrent rise time and slow decay time, if we want to fulfill the conditions above, the temporal intensity profile of the gating pulse $I_g(t)$ must as shorter as possible to achieve delta-function like gating function.

4.2 Analysis of Several Different Samples utilize Chirp-Controlled THz-TDS

In order to discuss the PC antenna sampling effect on THz time-domain spectroscopy, we prepare 3 samples to study this effect. (1) Metal Hole Array (MHA), (2) Lactose, and (3) Quartz, which have different properties in the THz range. MHA is a 2 dimensional photonic crystal which is used as band-pass filter in the THz region [4]. Lactose, which has a significant absorption in the THz region [5]. Quartz, which has flat response in the THz region, is the most favor material used as substrate in many applications.   The experimental setup is same as Figure 3-12.
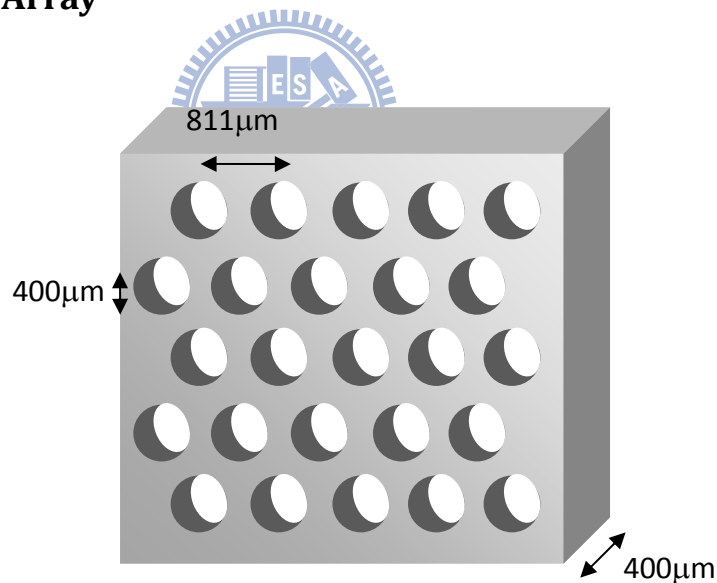
4.2.1 Metal Hole Array

Figure 4-2 Schematic of metal hole array.

Figure 4-2 shows the schematic diagram of our MHA sample, which is a two dimensional photonic crystal array of hexagonal lattice. The diameter of the hole is about 400   m, period 811mm, and thickness 400   m, which leads to central transmittance frequency around 0.42 THz.
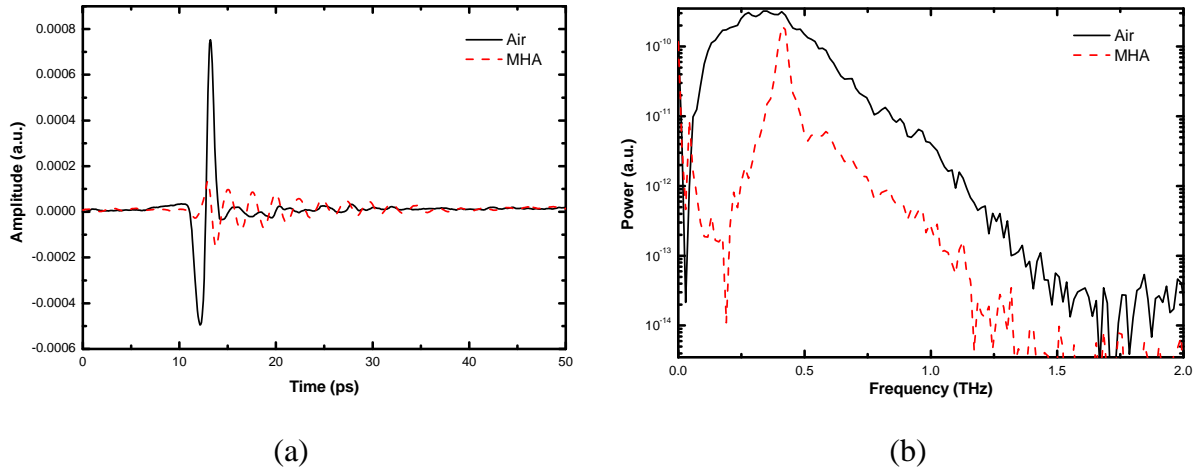
(a)   (b)

Figure 4-3 (a) Time domain profile of reference THz field and the THz field which pass
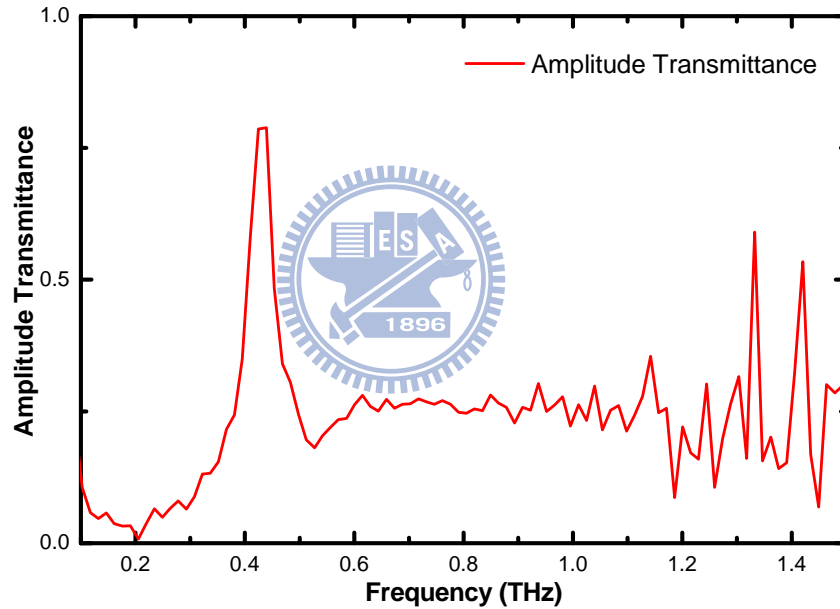
through MHA, (b) power spectrum.

Figure 4-4 Amplitude transmittance of MHA.

Figure 4-3 (a) shows the measured time domain profile of signal and reference field, the

pump power and probe power of the laser pulse is 30mW, 20mW respectively, the pump pulse

and probe pulse are compressed to TLP with SLM, so the pump pulse and probe pulse are

both zero chirp in the experiment. Figure 4-4 is the corresponding amplitude transmittance of

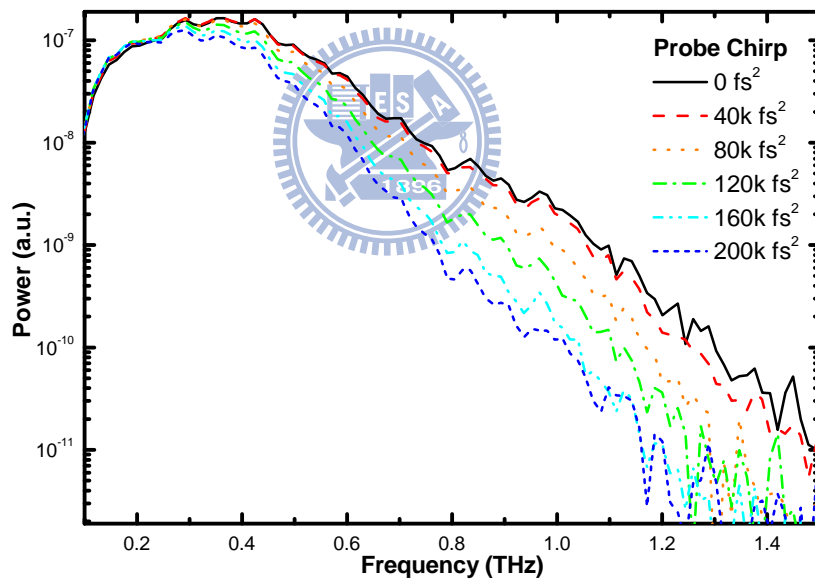MHA, which shows a maximum transmittance at 0.425 THz.

(a)
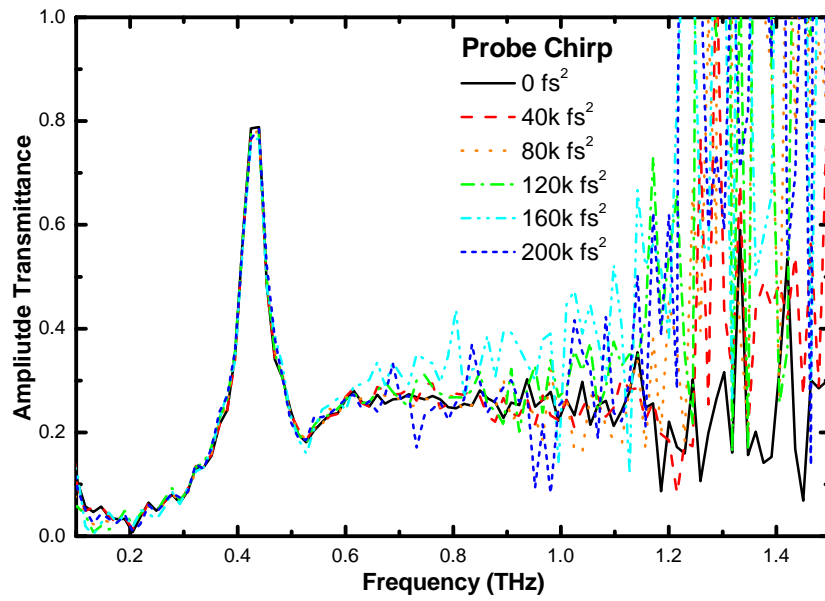
(b)

Figure 4-5 (a) Amplitude Transmittance of MHA with different gating pulse, and (b) the

corresponding power spectrum of reference signal.

Figure 4-5 shows the experimental results of MHA transmittance under different probe

pulses with different chirp. We can find out the transfer function remains unchanged through

0.2~0.6THz under different probe pulse, however, the transfer function shows strong

distortion beyond 0.6THz.

4.2.2 Lactose

(a)   (b)
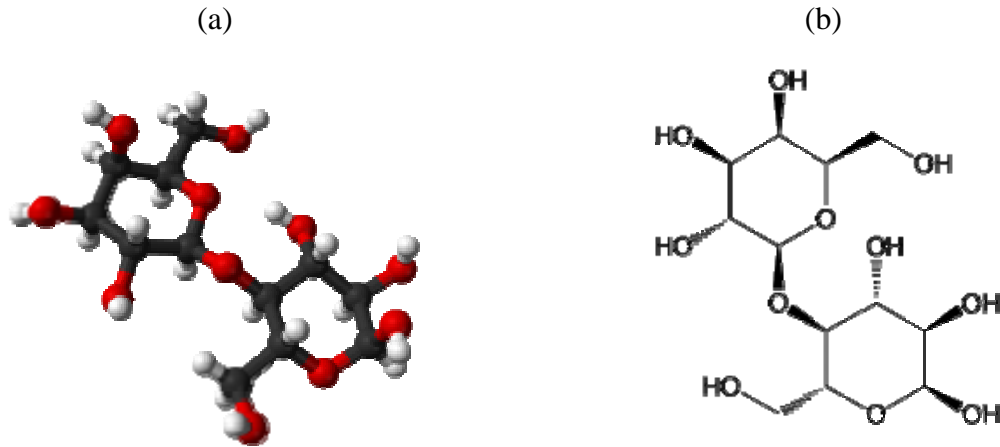

Figure 4-6 Molecule structure of lactose.

Lactose is found most notably in milk, which is also called milk sugar. The molecule structure of lactose is shown in Figure 4-6 (b). The vibration frequency of OH-bonds leads to absorption in 0.53THz.
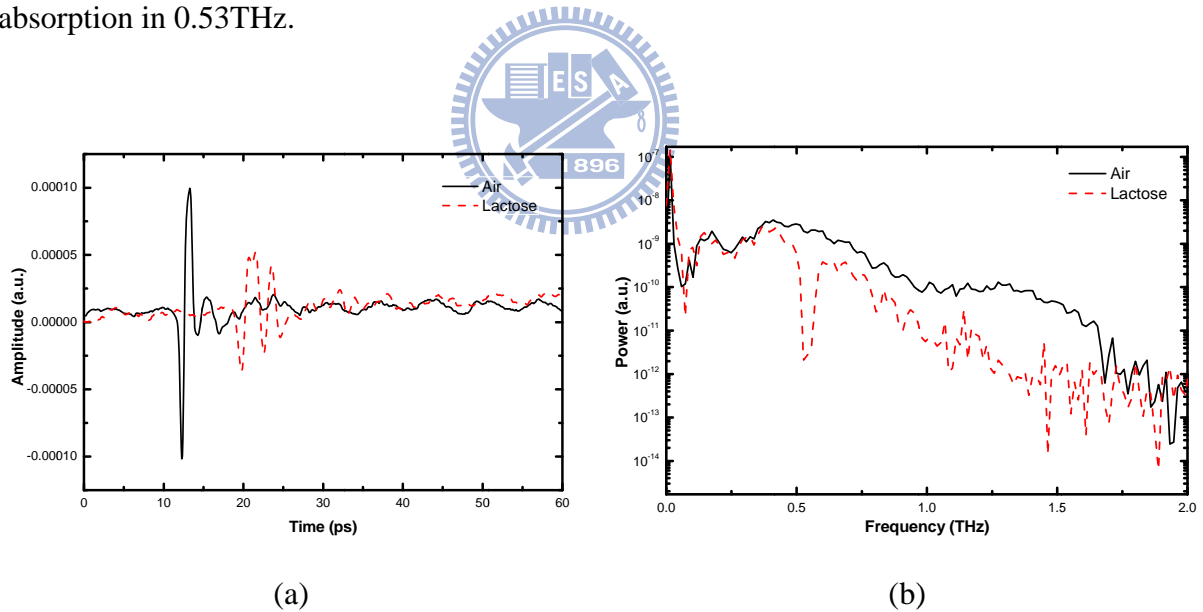

(a)   (b)

Figure 4-7 (a) Time domain profile of reference THz field and the THz field which pass through lactose, (b) power spectrum.

Figure 4-7 (a) shows the time domain profile of signal field and reference field, and (b) the correspond power spectrum. The pump power is 30mW, and probe power is 20mW, pump pulse and probe pulse are both zero chirp.
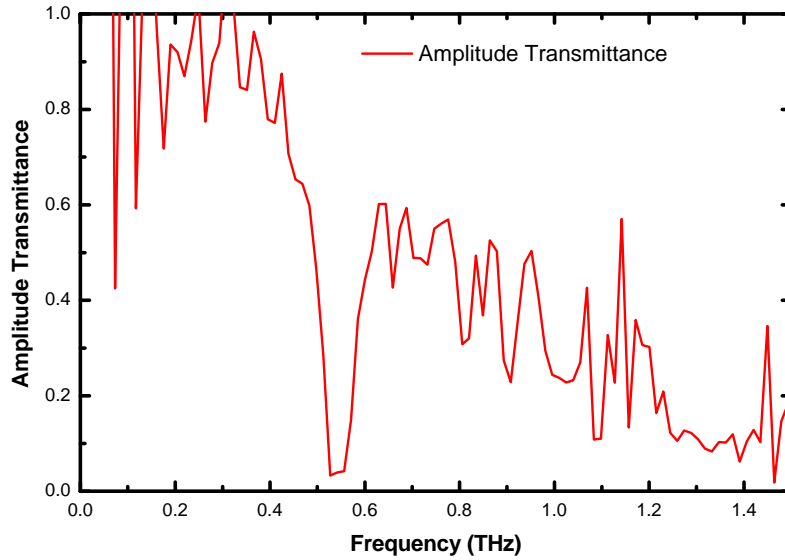
Figure 4-8 Amplitude transmittance of lactose.

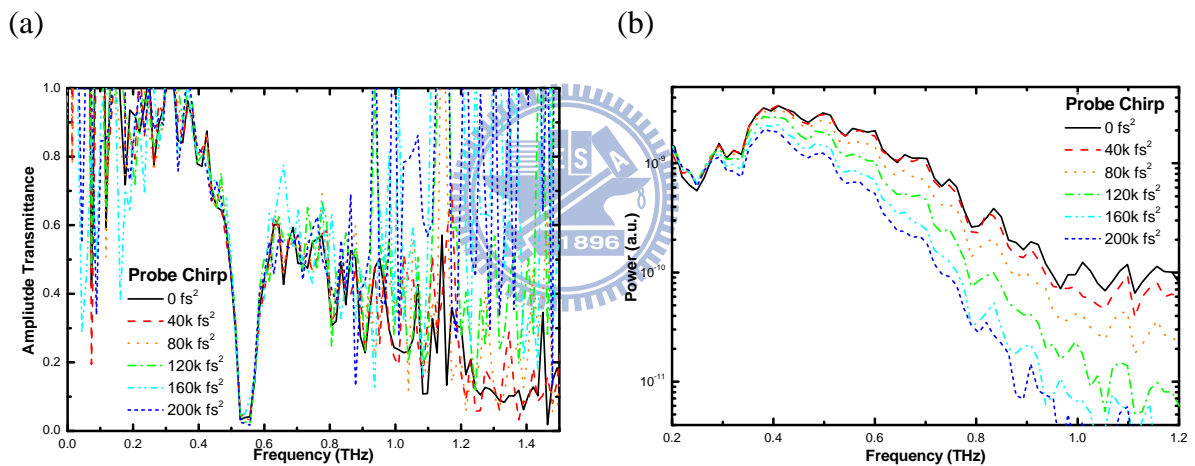(a)   (b)

Figure 4-9 (a) Amplitude Transmittance of lactose with different gating pulse, and (b) the

corresponding power spectrum of reference signal.

The amplitude transmittance of lactose is shown in Figure 4-8, the maximum absorption

peak is located at 0.527 THz. Figure 4-9 shows the amplitude transmittance under different

probe pulse, the absorption peak is also remains unchanged from 0.4THz to 0.6THz. However,

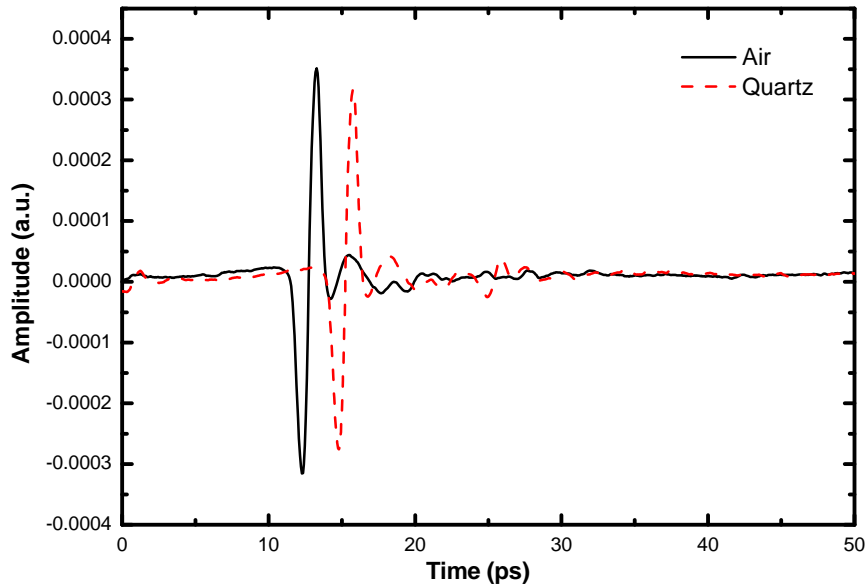it shows a strong distortion below 0.4THz and beyond 0.6THz.

4.2.3 Quartz

Figure 4-10 Time domain profile of reference THz field and the THz field which pass through a 0.7mm quartz.
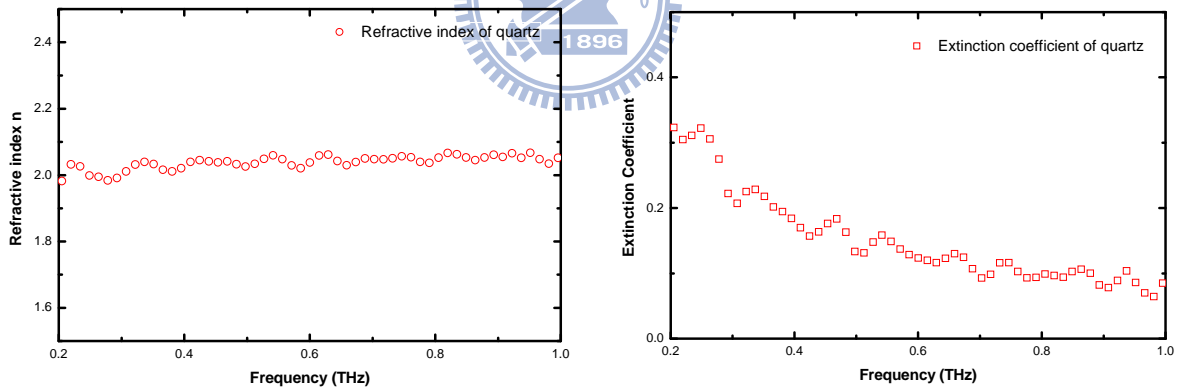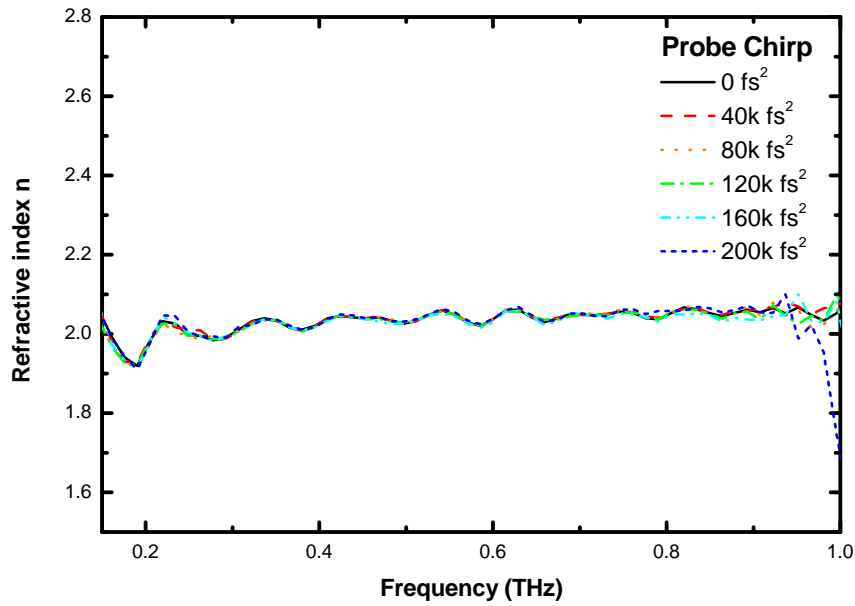

Figure 4-11 (a) Refractive index of quartz, and (b) extinction coefficient of quartz.

Figure 4-10 shows the time-domain profile of signal and reference field, and refractive index and extinction coefficient can be calculated with equation (4.10) and (4.11) respectively, the results are shown in Figure 4-11. The refractive index is about 2 in the THz range.

(a)

(b)
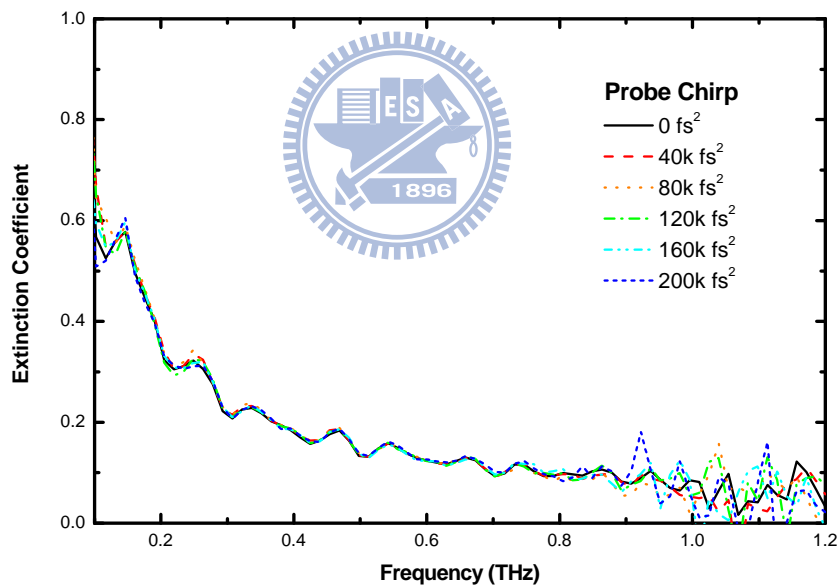
Figure 4-12 Refractive index and extinction coefficient of quartz under different probe pulses.

The calculated refractive index and extinction coefficient under different probe pulses are shown in Figure 4-12, the experiment results shows extreme different than the measured results of MHA and lactose. The refractive index and extinction coefficient remains unchanged with different probe pulses, the possible results are discussed below.

4.3 Material Optical Constant Measurement Uncertainties Due to the Chirp of Laser

From the experimental results above, we can find out the transfer function of MHA and lactose will be distorted under strong chirped pulses, however the chirp pulse wouldn't change the transfer function of quartz, which has flat response in the THz range. The reason that the transfer function of MHA and lactose show strong distortion is the "correlation process" of the THz field and the time-dependent conductance, which is discussed in chapter 4.1.2. The major feature of these two samples is band pass filter with center frequency 0.42THz and strong absorption at 0.53THz, it remains unchanged under different gating pulse.

However, the refractive index and extinction coefficient of quartz remain unchanged in the efficient THz bandwidth range, why it shows extreme different behavior than the other two sample? It may contribute to two reasons :

(1) The complex dielectric function of quartz remains constant in the terahertz range where we want to study, so it doesn't matter to the chirp of probe pulse.

(2) When the probe pulse with higher chirp, it means the pulse duration is enlarged in time, recalled the time-dependence conductance again :

$$g(t) = \int^t dt' I_g(t') \left(1 - e^{-\frac{(t-t')}{\tau_s}} \right) e^{-\frac{(t-t')}{\tau_c}} \tag{2.24}$$

We can simulated the time-dependence conductance under different pulse width, the results are shown in Figure 4-13 :
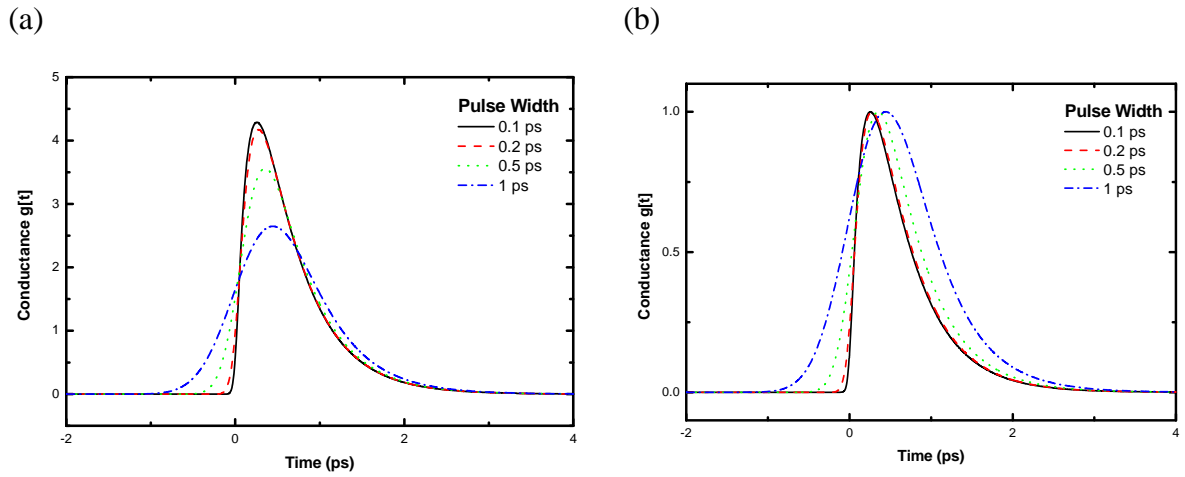
Figure 4-13 (a) Time dependent conductance g(t) at gating pulse width of 0.1ps, 0.2ps, 0.5ps and 1ps, (b) normalized the peak value to 1.

From the simulation results above, we can found out that the time-domain profile of the conductance will transfer from asymmetry shape to symmetry, the symmetry profile of the gating function in time-domain will transfer the correlation effect to convolution, and eliminate the correlation effects, as discussed in section 4.1.2.

4.4 Conclusion

In this chapter, we measured three samples with different properties in the THz range we want to study. The photoconductive antenna sampling effect is well discussed in theory and experiment. It can help us understanding the reliability of terahertz time domain spectroscopy.

We found out the transfer function of THz-TDS will remains unchanged under very strong chirped pulse, although the strong chirped gating pulse will reduced the measured THz power, however, the strong chirped pulse with longer pulse duration will transfer the time-dependence conductance into symmetry profile, which will reduce the sampling effect. In the zero chirped probe pulse case, the delta-function like shape of the gating function will also eliminates the sampling effect, and with higher SNR. So in the experiment of THz-TDS, the zero-chirped pulse is suggested in the experiment.

References

[1] L. Duvillaret, F. Garet, and J.L. Coutaz, "A reliable method for extraction of material parameters in terahertz time-domain spectroscopy," IEEE J. STQE., Vol. 2, pp. 739-746, Sep., 1996.

[2] T.D. Dorney, R.G. Baraniuk, and D.M. Mittleman, "Material parameter estimation with terahertz time-domain spectroscopy," J. Opt. Soc. Am. A, Vol. 18, pp. 1562-1571, Jul., 2001.

[3] I. Pupeza, R. Wilk, and M. Koch, "Highly accurate optical material parameter determination with THz time-domain spectroscopy," Opt. Express, Vol. 15, pp. 4335-4350, Apr., 2007.

[4] D. Qu, D. Grischkowsky, and Weili Zhang, "Terahertz transmission properties of thin, subwavelength metallic hole arrays," Opt. Lett., Vol. 29, pp. 896-898, Apr., 2004.

[5] E.R. Brown, J.E. Bjarnason, A.M. Fedor, and T.M. Korter, "On the strong and narrow absorption signature in lactose at 0.53THz," App. Phys. Lett., Vol. 90, pp. 061908-1 -061908-3, 2007.

Chapter 5 Future Works

5.1 Summation of this work

In this work, we study the THz generation and detection mechanism of PC antennas with femtosecond pulse shaping technology, which help us understand the role of chirp in the generation and detection processes. The influence of carrier life time and momentum relaxation in material is also studied by the simulation with one dimensional Drude-Lorentz model, it gave us the information about how to choose suitable materials as emitter or detector in different kinds of THz applications. The summation of suitable emitter and detector materials were shown in Table2-2 and Table 2-3 respectively.

In the application of THz-Time Domain Spectroscopy, the PC antenna sampling effect is also discussed, experiment results found that the strong chirped probe pulse will results into a symmetry profile of time-dependence conductance, it can eliminate the correlation effects of PC antenna.

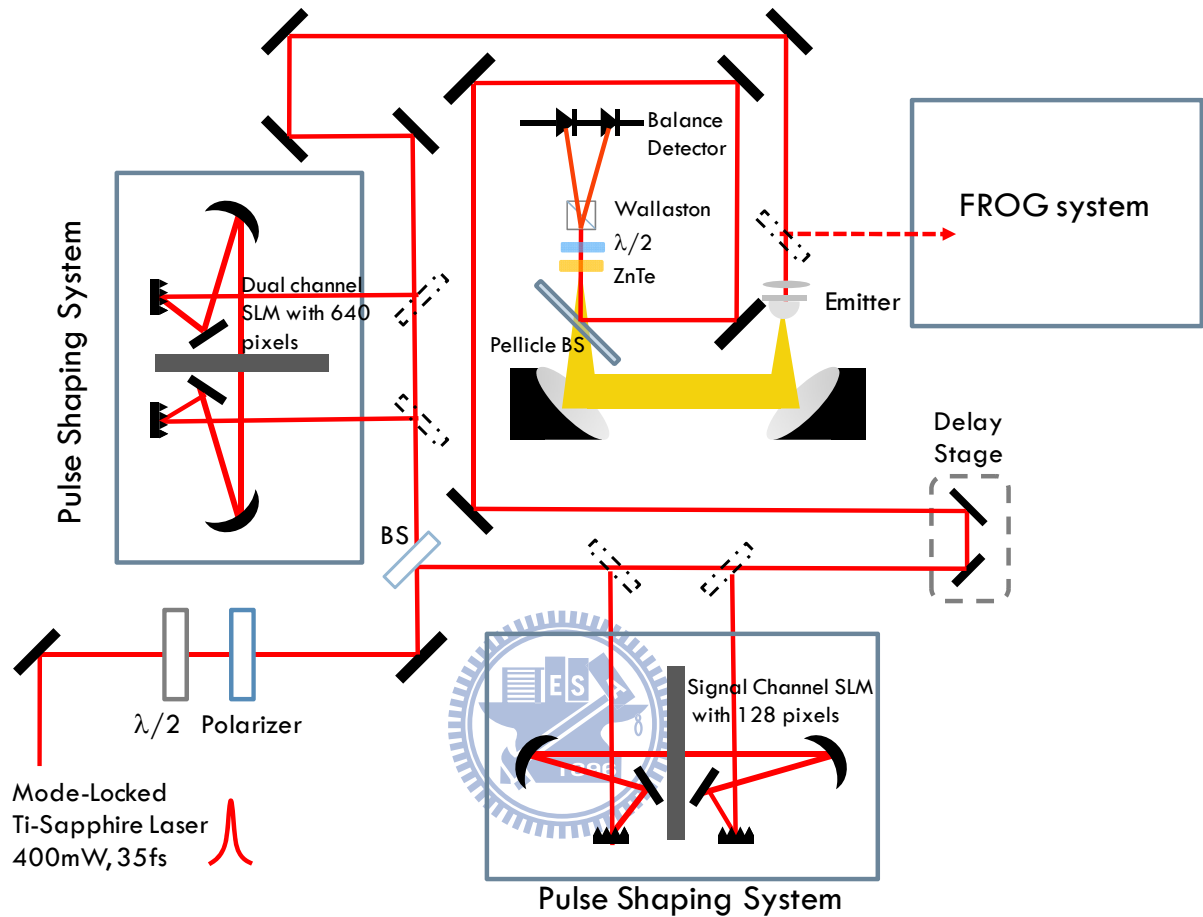## 5.2 Coherent-Controlled Narrow Band to Broad Band THz Spectrometer

Figure 5-1 Schematic layout of coherent-controlled narrow band to broad band THz time domain spectrometer.

Figure 5-1 shows the suggested tunable THz Time domain system, which composed with two pulse shaping system, the SLM used to control pump pulse is a dual-channel SLM with 640 pixels, which can provide amplitude and phase modulation simultaneously, with such a dual channel shaper, first, we can also compress the pump pulse into TL-pulse, which can generated THz field with broadest spectrum, and the gating pulse is pass through another pulse shaper, which is also used to compress the gating pulse to achieve delta-function like

gating function. The detection mechanism is EO-sampling, which can achieve maximum bandwidth detection and reduce the PC antenna sampling effect.

Such a system can be worked on two modes : (1) broad band mode, and (2) narrow band mode. For traditional application of broad-band detection, the pump pulse and probe pulse can also be compressed to zero chirp, and can achieve both maximum emission efficiency and detection efficiency. For the application of narrow-band mode, we can use this dual-channel SLM to generate multi-pulses [1], which can generated tunable-narrow band THz pulses. This narrow-band THz source can be used in the application of absorption spectroscopy, which will have higher sensitivity than broad band sources.
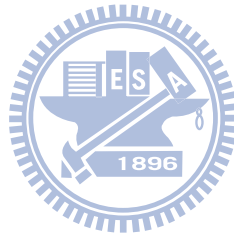
References

[1] Shin-Cheng Liu, "The Applications of Pulse Shaping in Ultra-broad Bandwidth Pulse

Characterization and Multi-pulse Generation," Master Thesis, NSYSU (2008).